Maria Sklodowska-Curie Actions (MSCA)
Innovative Training Networks (ITN)
H2020-MSCA-ITN-2018
Grant number 813137

Project number 813137

URBASIS-EU
New challenges for Urban Engineering Seismology

DELIVERABLE

Work Package: WP3
Number: D3.1 – General guidelines to assess soil response in urban areas

Authors:	**Janusz, Paulina**	(ETHZ)
Co-authors:	Fäh, Donat	(ETHZ)
	Perron, Vincent	(ETHZ)
Reviewer	Bonilla, Luis Fabian	(UGE)

Approval	Management Board
Status	Final Version
Dissemination level	Public
Delivery deadline	30.09.2021
Submission date	30.09.2021
Intranet path	https://urbasis-eu.osug.fr/Scientific-Reports-157

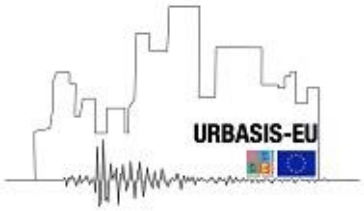

Contents

1. Introduction and outline

Near-surface geological structures are known to modify ground motion in terms of amplitude, duration, and spatial variability. Particularly, seismic waves can be significantly amplified in thick and soft sedimentary basins. The significance of the site effects is evidenced, among others, by the San Francisco earthquake of 1906, the Loma Prieta earthquake of 1989, and the Mexico earthquake of 1985 (Figure 1). In all examples, the severity of the damage was significantly increased due to local geological conditions (Bard, 1997). Therefore, it is essential to estimate the influence of the local site effects when assessing seismic hazard and risk (Poggi & Fäh, 2016). By characterizing the local geological structure, evaluating geophysical and geotechnical parameters, and estimating soil amplification at a given location, we can better understand the spatial variability of ground motions and perform more reliable simulations for different earthquake scenarios, as well as reduce uncertainty in ground motion predictions (Poggi & Fäh, 2016). Cities are particularly susceptible to earthquake risks due to the accumulation of infrastructure and high population density. The concentration of wealth and rapid urbanisation in urban areas have significantly increased the seismic risk, even in countries characterized by low to moderate seismicity. It is therefore important to assess the intensity and variability of the soil response in order to plan appropriate mitigation and risk reduction strategies.

In the first part of the report (chapters 2, 3, and 4), I would focus on general information about site effects, case study area, and the methods for estimating site response, concentrating on the specifics of an urban environment. For more detailed information about different strategies for microzonation and site characterization, the reader is referred to Poggi & Fäh, (2016) which contains an extensive overview of the topic. In the following report, I intend to summarize some of the issues included there but also supplement them with information about some of the techniques introduced or developed recently. I will also provide more insight into the specifics of an urban environment and focus on the experiences I gained while working in the Lucerne area. However, the following report is a selection; I do not plan to cover the vast topic of site response analysis and techniques for site characterization in urban areas. I will focus mostly on methods that I used in the city of Lucerne but I will provide also a short overview of the usage of other geophysical methods, numerical modelling, and nonlinear soil behaviour analysis to show a more detailed overview of the method and procedures that are used in the research community. A detailed report about the current developments in the topic of nonlinear site response will be published next year (ESR3.1 URBASIS Deliverable 2).

In the second part (chapter 5), I will show the detailed results of some of the described techniques applied in the city of Lucerne located in central Switzerland. Some preliminary microzonation analyses (Poggi et al., 2012a) and site characterization campaigns (Michel et al., 2013; Poggi et al., 2013b) were performed there in the past. In my PhD project, we would like to perform a detailed site response analysis for the Lucerne area considering both linear and non-linear soil behaviour. I will demonstrate some practical aspects and challenges encountered during our study in a densely populated middle-size city located in a low-seismicity area. We have applied empirical and passive seismic methods to estimate directly the amplification factors in the area. We will use also site proxies that allows getting indirect information about site response. In the next step, we plan to build a 3D geophysical model of

the area and study the site response using numerical methods. To evaluate the geometry of the basin and shear wave velocity structure, we take advantage among other of the non-reference techniques such as H/V and passive seismic methods. Our aim is to characterize the basin up to the bedrock. The investigations in the Lucerne area are still in progress.

In the following report, details of applying empirical methods and ambient vibration to assess directly amplification will be shown. In addition, I will present examples of the procedure and result of passive array measurements, as well as the process of mapping the fundamental resonance frequency across the area.

In the last part (chapter 6), the reader can find a short summary.

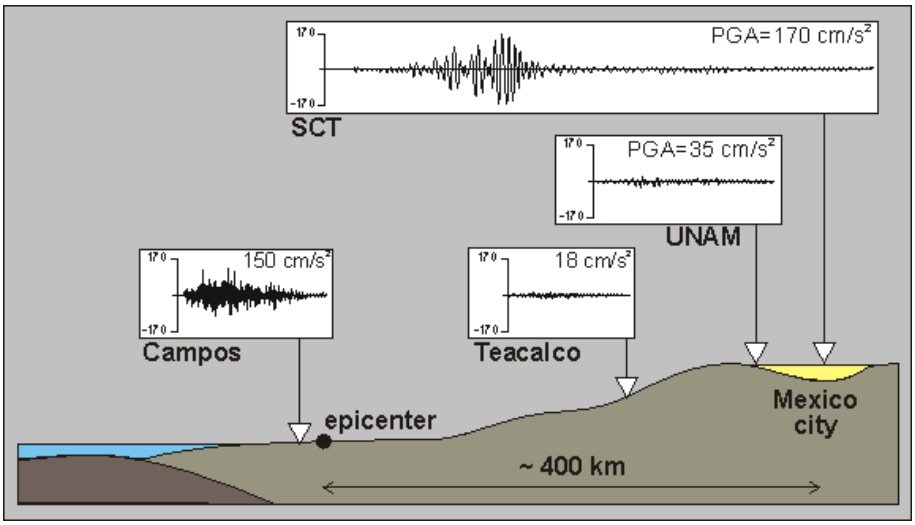

Figure 1. Site effects in Mexico City in 1985. The amplitude of surface waves was greatly enhanced by local geological conditions. Source: Çelebi et al. (1987)

2. Site effects

The term "seismic site effects" involves different phenomena. Strong seismic impedance contrast between bedrock and sediments is an important factor in amplifying the earthquake signal, as well as trapping and constructive interference of seismic waves (Bard, 1997). Large amplification factors are often observed in sedimentary basins with complicated geometry because of the generation of complex 2D or 3D resonance patterns (Roten et al., 2006). Edge-generated surface waves developed at the basin borders are visible on earthquake recordings as a long-duration surface-wave train and can contribute to devastating damage (Michel et al., 2014). The influence of surface topography has been also investigated (Bard, 1997) showing amplification over convex and de-amplification over concave topography, however, the effect of topography on amplification is generally not very significant (e.g. Burjánek et al., 2014a; Burjánek et al., 2014b) when compared to the effects induced by sediments and weathering. Not all phenomena affecting the seismic waves can be fully explained by the elasticity theory. The intrinsic attenuation and energy scattering of seismic waves during propagation are also important factors controlling the ground-motion amplitude and duration.

For strong motion, we also need to consider non-linear soil behaviour (e.g. Beresnev and Wen, 1996; Bonilla et al., 2005; Roten et al., 2009). Above some strain level, the damping ratio rises and the shear modulus decreases with increasing strain amplitude (Beresnev & Wen, 1996). The shear wave velocity and the soil fundamental frequency decrease simultaneously due to the reduction of the shear modulus (Beresnev & Wen, 1996; Roten et al., 2009). While the S-wave velocity reduction at high-strain levels may cause amplification, usually the contribution of the increased attenuation prevails, reducing amplitude, or even causing de-amplification at high frequency during strong motion (e.g. Roten et al., 2009). At low frequency, however, non-linearity is mostly causing amplification because of the reduction of the soil fundamental frequency. Moreover, some authors suggested that dilatant soils can recover momentarily the shear strength triggering large deformation (Bonilla et al., 2005).

In addition, during strong shaking, sudden increase of sediments pore pressure may result in temporal total loss of strength of the soils that start to behave like a fluid. The phenomenon is called liquefaction and can result in serious damage to the buildings (Kramer, 1996). Other secondary phenomena induced by the earthquake, including earthquake-triggered flooding (e.g. tsunami, seiche) and ground failure (e.g. landslides, rock falls, subsidence) can be similarly disastrous.

3. Case study: Lucerne

3.1 Geology

Lucerne is a middle-size densely populated city in central Switzerland. It is characterized by low-to-moderate seismicity (Figure 3) and is located on a basin filled with unconsolidated Quaternary fluvio-lacustrine deposits. The underlying bedrock comprises clastic sedimentary rocks, mainly hard sandstones, siltstones, and mudstones, deposited in the subalpine Molasse basin (Figure 2). The inter-and intraglacial processes are responsible for forming a complex-shaped basin and deposition of glacial moraines with different thicknesses. Basin infill consists mostly of interspersed layers of sand, gravel, clay, and silt unevenly distributed across the basin (Keller + Lorenz AG, 2010; Poggi et al., 2012a). Such predominantly very soft deposits are classified as D, C, and F category (e.g. Keller + Lorenz AG, 2010) of the Swiss Building Code classification (SIA, 2020). Moreover, the water table is generally shallow, not exceeding 5m across the basin (Geoportal Kanton Luzern, 2020; Poggi et al., 2012a) contributing to the risk of liquefaction.

3.2 Seismicity and vulnerability

During the last 50 years, the seismicity in central Switzerland has been low (Gisler et al., 2004). However, in the past, the area was struck by several strong earthquakes, including 1601 (Mw 5.9) and 1774 (Mw 5.7) events and swarms in 1777 (maximum Mw 5.1) and 1964 (maximum Mw 5.3) (Fäh et al., 2011; Gisler et al., 2004) (Figure 3). Moreover, the evidence for three even larger paleo-events in central Switzerland (Mw 6.5-7.0) was found (Strasser et al., 2006).

The damage caused by the 1601 earthquake which is the strongest historical event in central Switzerland in the past millennium and one of the strongest events in the whole of Switzerland (Schwarz-Zanetti et al., 2003) is described in detail by historical sources. The so-called “little

town" which today is a part of historical Lucerne's old town (Figure 4) was the most affected, including some serious damage to the city walls. The earthquake produced rock falls at many places, e.g. at Mt Bürgenstock, and triggered subaquatic landslides resulting in a 4-5 m-high tsunami (Schnellmann et al., 2002, 2004; Siegenthaler et al., 1987; Strasser et al., 2006). The riverbed of the river Reuss in Lucerne was 6 times emptied and filled again due to seiche (Schwarz-Zanetti et al., 2003). Today, densely populated urban and suburban areas cover a much bigger part of the basin than in 1601, which greatly enhances seismic risk and city vulnerability (Poggi et al., 2012a) if such a strong earthquake repeats.

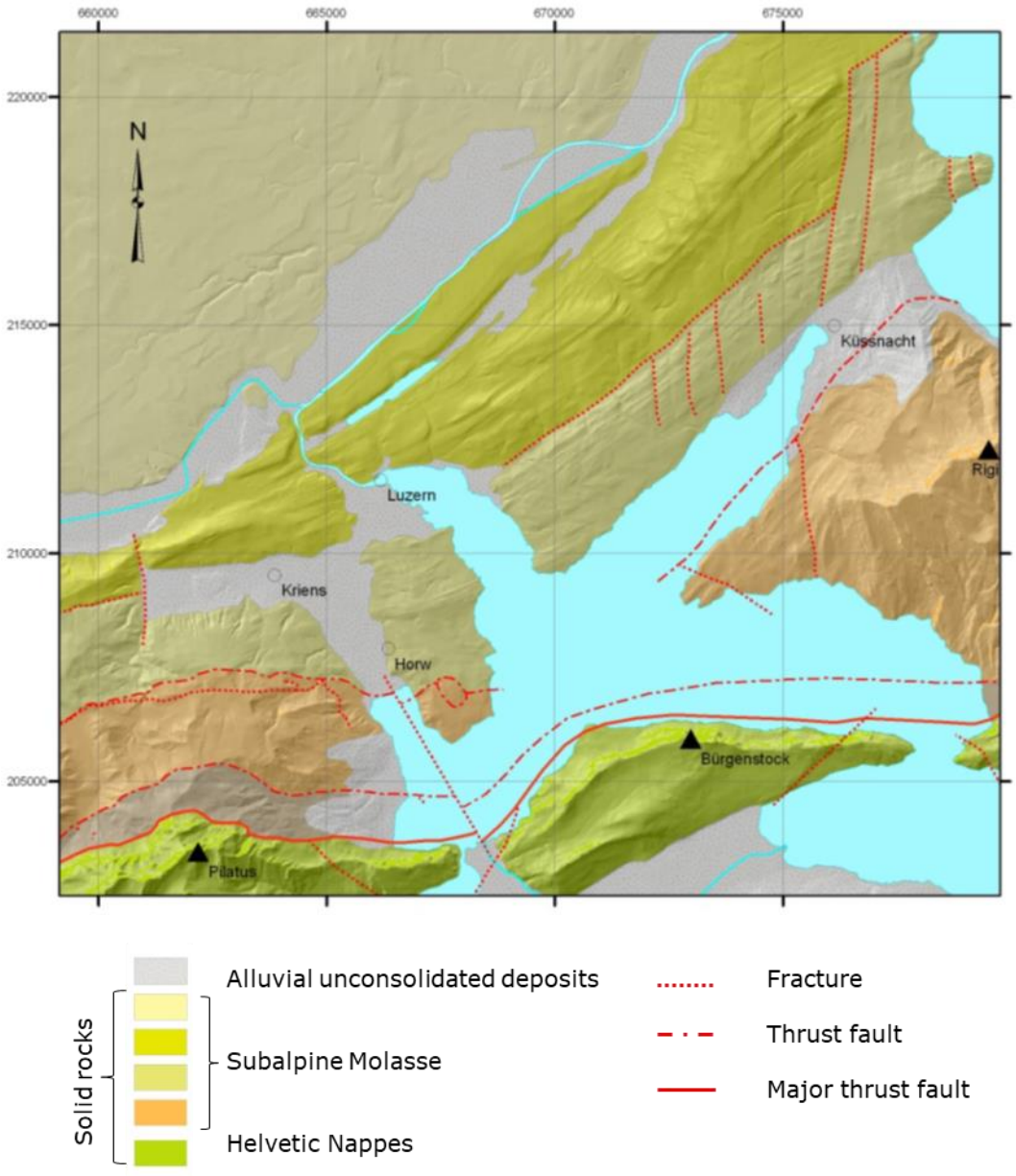

Figure 2. Simplified tectonic map of Lucerne area. Modified from Keller + Lorenz AG, (2010)

3.3 Challenges

The city of Lucerne provides us with a challenging case study. The complex basin geometry and high impedance contrast between bedrock and soft sedimentary infill suggest that both 2D and 3D resonances should be considered in site effects analysis. Moreover, non-linear soil behaviour is suspected of playing an important role during strong events. Last but not least, local geology is characterized by significant lateral variability at small scales. Site response assessment in such a complex area requires detailed geotechnical and geological data and a dense network of high-quality geophysical measurements. Besides, the ambient noise level in Lucerne is high and strongly variable over space and time.

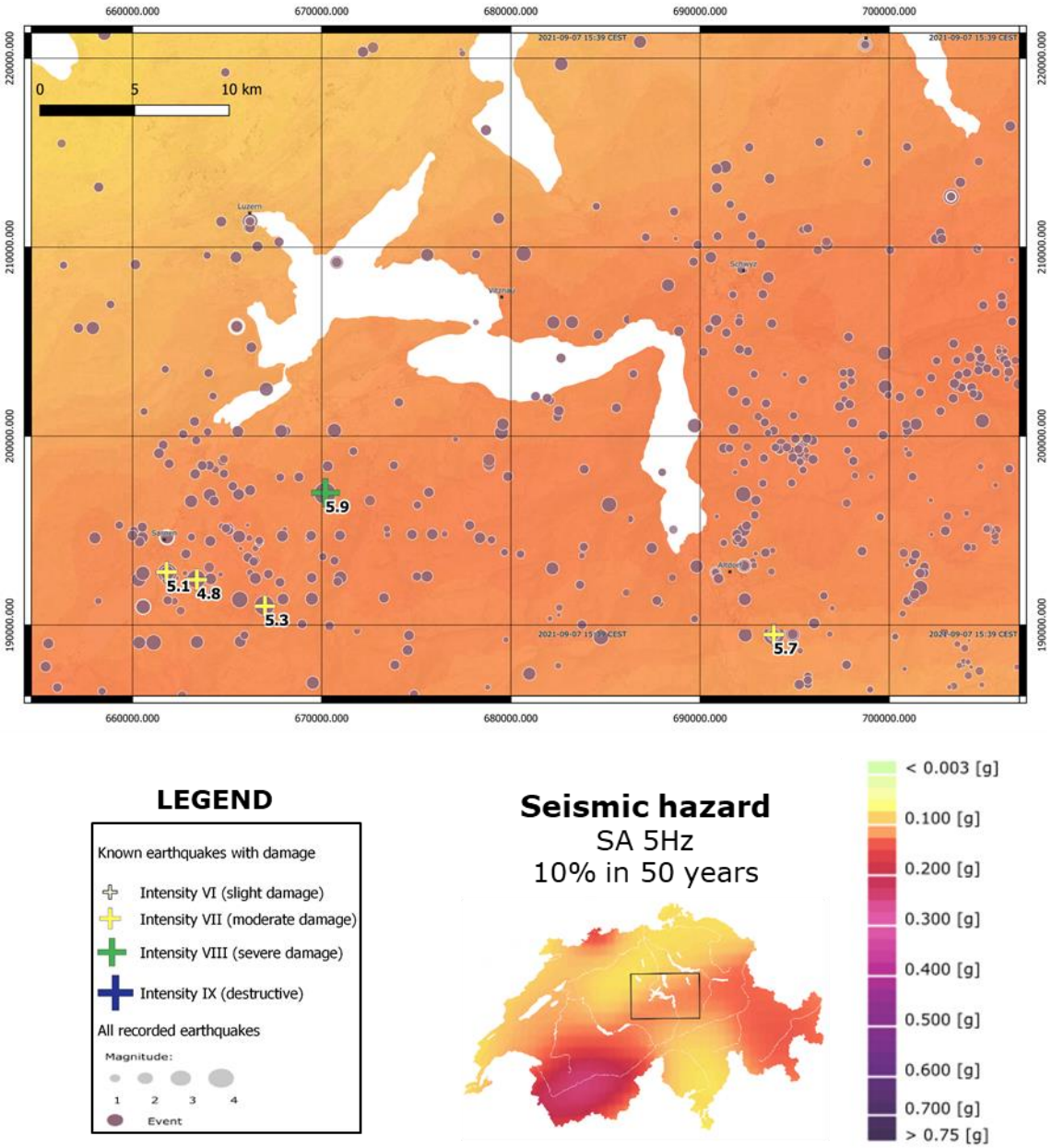

Figure 3. Seismic hazard for Switzerland for PGA and a return period of 475 years. Lucerne Lake area marked with rectangular is located in low-to-moderate seismicity area. All recorded (circles) and strong earthquakes(crosses with magnitude) are marked. Modified from Swiss Seismological Service (SED), (2021)

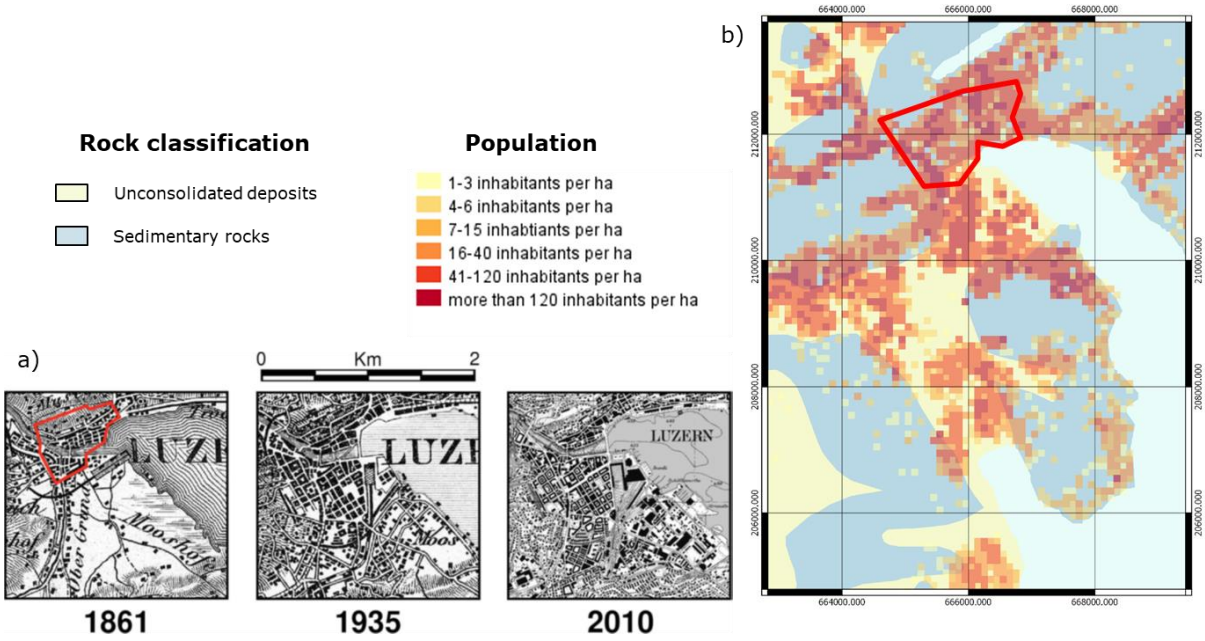

Figure 4. a) Urbanization in Lucerne basin, on the first map – the red area indicates the possible borders of the old city in 1601 (Poggi et al., 2012a). b) Current population density in Lucerne and juxtaposed with dominating geology. Base maps source: Federal Office of Topography Swisstopo, (2021).

4. Methods for site response analysis

4.1 Introduction

The goal of site response analysis is a quantification of the ground-motion amplification including consideration of its spatial variability and in effect, a definition of the site-specific hazard and reducing the uncertainty of ground-motion predictions.

Typically, the first step of site response analysis is to collect all available data related to the considered area, focusing on geological, geotechnical, and geophysical parameters. Such information allows planning effective measurements campaigns, discovering vulnerable areas, and identifying potential areas with large site effects.

Amplification can be estimated directly using empirical and passive seismic methods such as reference site techniques (Bard, 1997, 1999) where strong and weak earthquake motion or ambient noise recorded at one station is compared to the reference station (often rock site) to obtain relative amplification factors at different frequencies. The choice of the reference site is crucial in estimating the local site response using reference site methods.

Moreover, site amplification can be predicted using a variety of indirect proxies and indicators. For example, non-reference approaches like the horizontal-to-vertical spectral ratios (HVSR) method can be used to determine qualitative information about site response (e.g. Bard, 1999; Edwards et al., 2013; Lermo & Chavez-Garcia, 1994; Perron et al., 2018a). Other popular proxies include the Vs30 value that can be evaluated for instance with seismic methods, as well as strictly geological or topographic indicators like slope.

Several numerical methods can be also applied to estimate site response (Bard, 1997, 1999) by simulating the wave propagation through the soil column (1D) or inside the basin (2D and 3D); however, the knowledge of spatial variability of the geophysical and geotechnical parameters in the investigated area is needed. Hence, the first step to use the numerical methods is to build the subsurface model. The most relevant parameters needed as the inputs are the geometry of the model, the compressional (V_p) and shear (V_s) wave velocity profiles, density (ρ), and attenuation quality factors (Q_p and Q_s) if the target is only linear soil response. Additional information about geotechnical parameters such as shear moduli and damping as a function of strain is necessary to consider non-linear soil behaviour in the model.

To estimate the properties needed to build a subsurface, model different geophysical techniques are commonly used to characterize the site, including active (e.g. MASW, refraction seismic) and passive seismic methods (e.g. array technique). The main goal of using those methods is to infer surface wave dispersion curves and then invert them to obtain the S-wave velocity profile. More information about soil geotechnical parameters needed in non-linear site response analysis can be obtained using invasive techniques, mainly laboratory measurements of recovered samples or cone penetration tests (CPT) which better reflect in-situ soil properties.

While designing a numerical experiment, it is important to determine if it is sufficient to assume a one-dimensional model (1D), in many cases 2D or even 3D models are required to represent fully the complexity of the spatial response. Another important aspect is the size of the area and the planned resolution of the model. While for relatively small models, the computational resources are often no longer a limitation; simulations for large regions are still demanding in terms of time and computer power. In addition, 3D simulations are still restricted to low frequencies (< 4 Hz) because of the sparse availability of geophysical and geotechnical parameters in the models.

The choice of the applied method and techniques depends on the geological variability and supposed complexity of the investigated area, its extent, as well as the significance of infrastructure and seismicity in the region, but first of all on available financial resources. That is why it is important to plan optimal and cost-efficient investigations for determining the linear and non-linear site response. The uncertainty of the model also depends on the amount of work performed, the fewer number of experiments, the higher the uncertainty is. In addition, the usage of many different methods helps to determine better the uncertainty. Therefore, the accuracy and resolution of the resulting site response model is a compromise between actual needs and available budget and time. It is especially important in an urban environment, where certain limitations apply. Site response analysis in densely populated urban areas and industrial environments can be challenging among others due to wavefield interaction with buildings and their foundations, limited access to some areas, and the lack of free-field space to perform measurements. Due to the intensified human activity in cities, the background noise level is often too high to record weak ground motion generated by distant or low magnitude earthquakes. In addition, the presence of strong transient noise sources hinders the usage of ambient noise methods. Therefore, site response analysis is usually more difficult and expensive in urban areas.

In the following subchapters, I will describe several methods that are used in the research community to directly assess site amplification and to characterize site properties. I will focus

on the methods that I applied in my case study; however, a short overview of other methods will be presented as well.

4.2 Empirical observations

Ground-motion observation can be used effectively to estimate the amplification. The spectral amplitude of ground-motion (U) at the site can be defined as the convolution of source function (S), path (P) including geometrical spreading and attenuation, local geological condition (H), and instrumental response (I):

$$U(f) = S(f) \cdot P(f) \cdot H(f) \cdot I(f)$$

A technique commonly used to retrieve the site effect component (H) is the standard spectral ratio (SSR) method (Borcherdt, 1970). If the hypocentral distance is much larger than the distance between two stations, it can be assumed that both the source and path components are the same for the two stations. Therefore, by comparing the Fourier amplitude spectra (FAS) of ground motions recorded for the same earthquake at the two stations, we can estimate the relative amplification factor as a function of frequency. Typically, a rock station is chosen as a reference assuming a negligible ground amplification. However, the assumption that rock is free of all local effects is incorrect – surface rock outcrops have site response of their own because they are subjected to weathering, cracking, etc. The seismic hazard referenced to local outcropping rock can be therefore underestimated (Steidl et al., 1996). That is why it is recommended to infer shear wave velocity profile at rock site using for example active or passive seismic measurements.

Another solution is the usage of bedrock borehole ground motion as a reference, however, the destructive interference of up-and down-going waves must be considered (Steidl et al., 1996). Surface-to-borehole methods are also expensive, mostly because of the drilling cost. Even if it is decided to perform drilling, boreholes are rarely achieving the bedrock depth, especially in the urban areas located in deep sedimentary basins. An example is borehole station SBUS by the Lucerne Lake (Figure 9) which due to the cost has only 100 m and does not reach the bedrock. We need also to measure rock properties at depth in order to compare different sites.

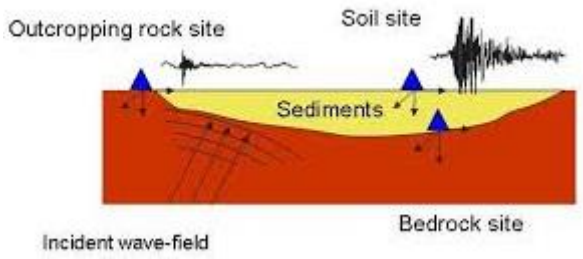

Figure 5. Scheme showing the location of seismic stations in the SSR method. Source: Parolai, (2012)

Another disadvantage of the SSR method is that it can only be applied to a small, dense network to ensure that the propagation component of ground motion is the same. To overcome this limitation, a generalised inversion scheme can be applied to multiple datasets to separate contributions from source, path, and site effect (e.g. Andrews, 1986; Bindi et al., 2009; Field and Jacob, 1995; Parolai et al., 2000). A similar approach developed by Edwards et al. (2013) is routinely applied to the stations of the Swiss seismic network (Figure 6) by the Swiss

Seismological Service (SED) (Michel et al., 2014) to obtain site amplification in relation to Swiss standard rock profile (Poggi et al., 2011). The Fourier spectrum for each event is modelled assuming the Brune source model (Brune, 1970) and considering regional geometrical decay and path attenuation (Edwards & Fäh, 2013a, 2013b) for each station and standard Swiss reference site. Then, it is assumed that the difference between measured and modelled spectrum is due to site effects allowing retrieving empirical amplification function (EAF). The method is applied to each local earthquake recorded by the network; the final amplification function is an average of the population of different site response realisations.

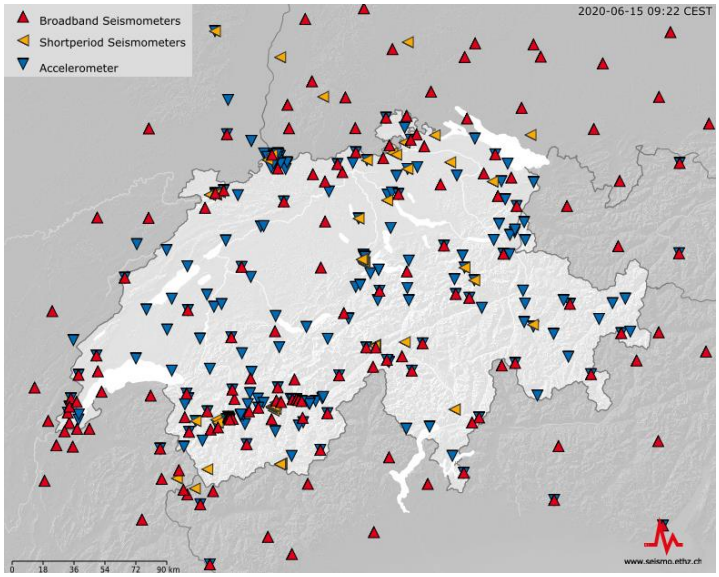

Figure 6. Swiss seismic monitoring network operated by Swiss Seismological Service (SED). Source: Swiss Seismological Service (SED), (2021)

The empirical approaches using earthquake recordings are commonly used for site response analysis. However, they may be difficult to apply in urban areas, especially when seismicity is low because their successful application requires collecting a statistically representative number of earthquakes with an adequate signal-to-noise ratio, which can be difficult in a noisy urban environment. For this reason, recording a sufficient number of earthquakes may require the deployment of instruments for several months or even years, which generates significant costs. Such a problem was encountered for example in the city of Lucerne. In addition, for installation for such a long period, permission and some agreement with the owners and local authorities must be established. In some cities, where the ownership is not so clear, it can be especially difficult. On top of it, secure places have to be found to ensure that the instruments are safe. We need to find sites where the stations can record with a relatively low level of disturbances and are far from the tall buildings or underground structures, which usually cannot be avoided in the areas of dense urban development.

In subchapter 5.2, the reader can find an example of using SSR and the EAF method in the city of Lucerne. I will show step by step the undertaken procedure including the details of the measurement campaign and data processing.

4.3 Non-invasive geophysical methods

Non-invasive geophysical techniques are the basis of site characterization allowing to non-directly obtaining information about soil structure and properties. While electrical, electromagnetic, magnetic, and gravimetric methods are sometimes used for example to map bedrock depth or groundwater table, the most suitable and popular are seismic methods because of the possibility of inferring the seismic wave velocities being one of the most important parameters while assessing site response. Seismic techniques can be divided into passive and active methods.

4.3.1 Active seismic

Although I did not perform the active seismic measurement campaign in the city of Lucerne and a real-life example will not be shown, the summary of the techniques is given below in order to present the full overview of different methods that are commonly used for site characterization.

The travel-time techniques (reflection and refraction seismic methods), based on measuring the time of wave propagation between the source and receivers, are sometimes used in site characterization to imagine complex structures with lateral velocity variations. The more popular approach is to perform a downhole seismic experiment where receivers are located in the borehole to retrieve the vertical velocity profile at the site.

The phase velocity dispersion function at high-frequency can be mapped using surface wave methods (i.e. SASW, MASW) (e.g. Foti et al., 2018; Lin et al., 2017; Park et al., 1999). The relative phase delays between receivers are analysed using, for example, the classical f-k approach (Lacoss et al., 1969) or t-f-k analysis (Poggi et al., 2013a) to retrieve dispersion characteristics of surface waves. Then, the dispersion curves can be inverted in order to obtain information about shear wave velocity at the site. A few MASW profiles were conducted in the past in the Lucerne area by company Resonance and Poggi et al., (2013a). We plan to use them to resolve better the shallower part of the subsurface; we will reprocess them to obtain dispersion curves, then inverted S-wave velocity profiles will be used while building a 3D model for the city of Lucerne.

Although passive seismic methods are often selected as a primary site characterization tool, active seismic is often used to resolve the shallower part of the subsurface. While passive methods allow characterizing deeper structures because low-frequency content (<10 Hz) dominates in ambient noise wavefield, the energy generated by active sources is concentrated above 10 Hz. In the urban areas where only low energetic sources such as a hammer can be utilized, the typical depth resolution of the active methods is only 20–40 m (Poggi & Fäh, 2016). Moreover, the high human-generated background noise level can effectively mask the useful signals and transient strong sources hinder the acquisition. Another issue is finding enough space to deploy a linear experimental setup.

Figure 7. MASW using hammer source during site characterization of seismic station belonging to Swiss Strong Motion Network (SSMNet) (Hobiger et al., 2021; Michel et al., 2014). Photo: Paulina Janusz

4.3.2 Passive seismic

The low-frequency part of the ambient noise wavefield (below 1 Hz) is related to natural phenomena, mainly of oceanic and meteorological origin. For shorter periods, the anthropomorphic sources prevail; the amplitude of ambient noise shows systematic variations due to the changing intensity of human activities (Bonnefoy-Claudet et al., 2006). Surface waves are shown to dominate the ambient noise wavefield at sediment sites (Bonnefoy-Claudet et al., 2006).

Different techniques based on ambient noise recordings have been developed to assess for example the site resonance frequency (H/V), to characterize the geophysical properties of the site such as shear wave velocity (array measurements), and sometimes to estimate directly the linear site response (noise-based spectral ratios).

High-resolving power, non-invasive character, and relatively low cost of the instruments deployments contribute to the popularity of the ambient noise-based techniques (Bonnefoy-Claudet et al., 2006; Poggi and Fäh, 2016). It is especially useful in urban areas where it is difficult to perform an active seismic experiment. On the contrary, ambient noise can be easily and rapidly recordable everywhere. Nevertheless, usage of ambient noise methods in urban areas is hindered due to the lack of free-field space to perform array measurements, the presence of strong transient sources of noise, effects of nearby structures and their foundations, etc.

Horizontal-to-vertical spectral ratios (HVSR)

Horizontal-to-vertical spectral ratios (HVSR) are a single station technique introduced first by Nogoshi & Igarashi, (1971) and then, revised and promoted by Nakamura, (1989). The procedure can be used with earthquake recordings (e.g. Chávez-García et al., 1996; Theodulidis et al., 1996) but the application to ambient noise is much more popular (e.g. Bard, 1999; Bonnefoy-Claudet et al., 2006; Lermo & Chavez-Garcia, 1994). Numerous experimental and theoretical studies demonstrated that the HVSR curve peak corresponds to fundamental resonance frequency f_0 of the site (e.g. Bonnefoy-Claudet et al., 2006; Fäh et al., 2001; Lermo & Chávez-García, 1993; Lermo & Chavez-Garcia, 1994). Hence, the HVSR method provides a simple and cheap tool for estimating the resonance frequencies of the site. However, it is not possible to directly interpret the HVSR amplitude as amplification factors (Bonilla et al., 1997; Perron et al., 2018a; Poggi & Fäh, 2016). Only the qualitative estimation of site response is possible using only the HVSR technique. In addition, using the H/V ratios to evaluate the damage distribution in the urban area is limited (Bonnefoy-Claudet et al., 2009).

The theoretical meaning of the HVSR curve has been a topic of heated dispute (e.g. Ansal, 2015; Bard, 1999). According to Nakamura, (1989), the S-wave resonance controls the shape of the HVSR curve but the most recent studies indicate the strong relation with Rayleigh-wave ellipticity (e. g. Fäh et al., 2001; Konno & Ohmachi, 1998). Including the Rayleigh-wave ellipticity curve in inversion together with surface wave dispersion curves can reduce the variability of the models (Fäh et al., 2003). Hence, H/V is often used to approximate the ellipticity function. However, the contribution of the Love-wave cannot be excluded (Bonnefoy-Claudet et al., 2008). The HVSR can be simply corrected by a factor $\frac{1}{\sqrt{2}}$ to remove the Love-wave contamination under the assumption that Rayleigh and Love-wave contribution to seismic noise is equal (Fäh et al., 2001, 2003). Another approach to recover the Rayleigh-wave ellipticity is to apply time-frequency analysis to single station ambient noise recording (Fäh et al., 2001; Poggi et al., 2012a). In this method, the signals are decomposed using a continuous wavelet transform and then Rayleigh wave contributions are identified under the assumption that the vertical component is free from the SH contribution. Finally, the H/V ratios are calculated only for the Rayleigh waves. An alternative method to estimate the Rayleigh wave ellipticity curve is the RayDec method (Hobiger et al., 2009) based on the random decrement technique. The idea of the technique is to add up a large number of specially adjusted horizontal and vertical signals what allows to emphasize the contribution from Rayleigh wave and suppress Love and body waves influence

More than one peak can be identified from the HVSR curve, each of them corresponding to different impedance contrasts in the subsurface. Assuming the horizontal layering, the fundamental resonance frequency constitutes an important constrain for the subsurface elastic properties what is shown by simplified equation (Kramer, 1996):

$$f_0 = \frac{V_s}{4h}$$

where V_s is the mean S-wave velocity of strata above the discontinuity and h is their thickness. By assuming the constant average velocity and that the peak indicates the bedrock-sediment interface, the HVSR method allows mapping the thickness of soft deposits over large areas (Poggi et al., 2012a). However, the resulting depth is often affected by large errors (Parolai,

2012). The reliability of such an approach strongly depends on the assumed velocity and correct identification of the peak. In addition, the results are not reliable in the basin with strong 2D and 3D resonance, the H/V peak is often very broad there (Bonnefoy-Claudet et al., 2009). The assumption that S-wave velocity increases with depth and there are no large lateral variations is also needed. Instead of using only the peak, in more sophisticated approaches, the whole curve is inverted together with the shear wave velocity profile (e.g. Poggi et al., 2012a).

If the f_0 value remains uniform across the basin, it may indicate a possibility of 2D/3D behaviour (Poggi & Fäh, 2016) in particular when azimuthal H/V ratios show the same polarization, often correlated with the basin orientation. Therefore, additional information about possible 2D resonances can be retrieved from single-station ambient noise recordings using polarization analysis (Burjánek et al., 2010). We have applied that method in the Lucerne area to check for any directional effects. However, the method does not show strong 2D resonances, even though; Lucerne is located in a deep glacial valley. More investigations will be performed in the future.

In subchapter 5.4, some applications of H/V ratios in the Lucerne area are shown, mainly mapping the fundamental frequency. In addition, an example showing that HVSR cannot be used directly as a measure of amplification is shown. The Rayleigh wave ellipticity curve from the RayDec method was also used in joint inversion with surface wave dispersion functions in order to obtain shear wave velocity structure in the Lucerne area (subchapter 5.5).

Ambient noise-based standard spectral ratios

In urban areas characterized by low seismicity and high background noise level, it is a challenge to record enough earthquakes with a good signal-to-noise ratio to reliably estimate the amplification factors using the SSR technique (Perron et al., 2018a). That is why, the equivalent methodology but applied to ambient noise (SSRn) was introduced (Field et al., 1990) in order to estimate the relative amplification factors. A similar assumption about the large distance to the vibration source needs to be adopted which is not guaranteed for the high-frequency part of the signal (Perron et al., 2018a). Several authors who investigated the applicability of the method demonstrated the SSRn method overestimates the amplification function (e.g. Çelebi et al., 1987; Field et al., 1990; Janusz et al., 2021a; Perron et al., 2018a). The example from the Lucerne area (subchapter 5.3) shows the clear overestimation of the amplification. Some studies show the shape of the SSR curve can be estimated to some extent using the SSRn method (e.g. Lermo & Chavez-Garcia, 1994; Yamanaka et al., 1993), however, in some cases only f_0 could be reliably assessed (e.g. Field et al., 1990; Lermo & Chavez-Garcia, 1994) or no correlation has been found (e.g. Field, 1996). The main reason that in some cases the results of the SSRn method are not convincing is the strong influence of the local sources, especially significant in urban areas. Therefore, the ambient noise wavefield and source distribution analysis is needed before using the SSRn technique in the site response assessment. It may be also beneficial to apply the method during the night when it can be assumed that sources that are more distant dominate the noise wavefield.

Because direct estimation of amplification using only ambient vibrations was shown to be unsuccessful, the hybrid approach combining SSR and SSRn methods (SSRh) was introduced by Perron et al., (2018a). In the first step, at least 2 two long-term monitoring stations, one on the rock and one in the basin, are deployed to record as many as possible earthquakes. Then,

the ambient noise is recorded at several sites in the basin to calculate noise-based spectral ratios (SSRn) between each site and long-term basin station. The resulting SSRn functions are then multiplied by earthquake-based SSR between long-term basin station and rock station (Figure 8).

As a result, the rock relative spectral ratio for each site is obtained. The SSRh has shown comparable results to the direct SSR evaluation on earthquakes for stations located in small sedimentary basins (Janusz et al., 2021a; Perron et al., 2018a). An example of a successful application of the method is the Lucerne area (subchapter 5.3). The method allows for high spatial resolution. What is essential in the low seismicity urban areas is that only a small seismic monitoring network needs to be deployed decreasing the cost of creating a high-resolution amplification model.

In subchapter 5.3, a detailed example of using both SSRn and SSRh in the Lucerne area is presented.

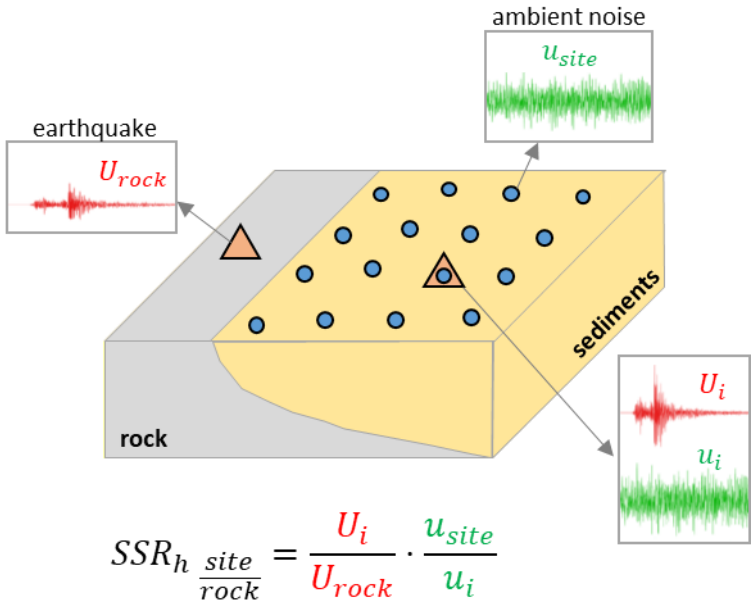

Figure 8. Schematic visualization of the SSRh method. U is earthquake ground motion and u is ambient noise.

Array technique

Another important passive seismic technique is an array method which is a multi-station spectral approach allowing to extract surface waves dispersion characteristics which can be then inverted for shear wave velocity structure (e.g. Kind et al., 2005). Array size, the configuration of the stations, recording time, and subsurface elastic properties are mainly responsible for array depth resolution (Jongmans et al., 2005). The performance of the methods is depending on the complexity of the local structure, the array configuration, and the ambient vibration wavefield (Chieppa, 2020). Both the quality and the resolution of the results are very sensitive to close transient noise sources (Poggi et al., 2012a). That is why it is preferred in an urban environment to perform measurements during the night. Furthermore, the determination of the location and orientation of the sensors should be very accurate (Jongmans et al., 2005), however, the abundance of ferromagnetic material in cities (train lines, electric power lines)

can increase the orientation error significantly (Poggi et al., 2012a). It is also critical to have enough free-field space to deploy the instruments; therefore, the typical instrumental configuration in urban areas is designed along the streets and open spaces like parks and gardens, which is not always the most optimal configuration.

Two groups of methods are commonly used to retrieve the phase-velocity dispersion curve from array recording: techniques based on the frequency-wavenumber analysis (Capon, 1969; Lacoss et al., 1969) and the spatial autocorrelation (Aki, 1957). While classical f-k methods utilize only vertical component and allow to obtain only Rayleigh wave dispersion, the three-component high resolution f-k method (Poggi et al., 2012a; Poggi & Fäh, 2010) based on high resolution f-k (Capon, 1969) uses all the three components which allow inferring both Rayleigh and Love dispersion curves as well as Rayleigh wave ellipticity. Including more dispersion curves during inversion helps to estimate the shear wave velocity with more confidence. However, the three-component high-resolution f-k fails to provide information about the sense of particle motion. The WaveDec method (Maranò et al., 2012, 2017) based on wavefield decomposition not only can distinguish between Rayleigh wave retrograde and prograde motion but also allows improving the accuracy of dispersion curves. The method uses maximum likelihood to estimate the wavefield parameters such as surface wave's velocities and direction of propagation.

In subchapter 5.5, the processing of array data is shown using examples from the Lucerne area. The procedure is presented starting from data preparation, initial processing to finding dispersion curves and inverting them to obtain shear wave velocity. For each step, a real-life example is presented. Because I did not perform array measurements in Lucerne by myself, the process of planning and performing the campaign is not described.

Ambient noise interferometry

Ambient noise interferometry can be used in site response studies in several applications, for instance, to better resolve subsurface velocity structure, to find attenuation model, or even to directly predict ground motion and amplification.

The idea of the interferometry is to reconstruct the Green's function between two points by cross-correlating the ambient noise recorded simultaneously on two receivers (e.g. Lobkis and Weaver, 2001; Prieto et al., 2011; Wapenaar and Fokkema, 2006). For more information about seismic interferometry, the reader is referred to Curtis et al., (2006) and Wapenaar et al., (2010a and 2010b). If the ambient noise wavefield is perfectly diffuse and equipartitioned, then the source is the Dirac delta function and the Green function represents the propagation term between the two stations, including the relative site response. The cross-correlation of seismic noise recordings was used by many authors to retrieve subsurface velocity structure at the local and regional scale (e.g. Lin et al., 2012; Picozzi et al., 2009; Schuster et al., 2004; Shapiro et al., 2005). Moreover, it was shown to be possible to recover the attenuation model using spatial coherency of ambient noise (e.g. Prieto et al., 2009, 2011). Seismic interferometry can be used also to study non-linear soil response (e.g. Bonilla et al., 2019; Chandra et al., 2016).

Some authors extracted the ambient noise impulse response function (ANIRF) between sites from seismic interferometry to predict the ground motion and ground amplification (e.g. Perron, 2017; Prieto et al., 2011; Prieto & Beroza, 2008; Viens et al., 2015). If one station is considered as a virtual source and signal is propagated through the network by cross correlating

the virtual source and each receiver, then, earthquake ground-motion propagation can be simulated. Several applications were shown including the possibility to map peak displacement (Prieto & Beroza, 2008) and pseudo-velocity spectra (Viens et al., 2015) or to estimate the amplification function (Perron, 2017). In that latter study, the SSR method was applied to virtual earthquakes, observing the same rules as in the case of a real event (e.g. epicentral distance much larger than stations distance, high signal-to-noise ratio). The study shows the possibility of quantitative prediction of site effects; however, the results are restricted to low frequencies and the underneath processing still needs to be investigated deeply before using the ANIRF more broadly in site response analysis.

We have tried to apply the ANIRF method following the approach described in Perron (2017). We used the data recorded by the temporary seismic network in Lucerne, as well as permanent velocimeters of SSMNet located around Lucerne Lake. However, for now, our attempts were not successful, only long-period correlations were obtained for frequency way below the site effect onset. The reasons for that may be either that the ambient vibration wavefield is uncorrelated due to many close-by sources in the city or the distances between the stations are too far to retrieve correlation at higher frequencies. Nevertheless, we plan to investigate the usage of interferometry in the city of Lucerne more deeply. Because we are still investigating the possibilities of the application of ambient noise interferometry and testing it to find the most optimal processing procedure, I decided not to show a detailed processing example. However, according to our experience until now, the main disadvantage of the methods based on seismic interferometry in an urban environment is a problem with an assumption that ambient vibration wavefield is fully diffuse because of the abundance of local strong noise sources which distribution usually is not uniform. For that reason, only cross-correlation of close-by stations can provide us with useful information in the frequency band suitable for analysing site effects (~1–3 Hz). For farther stations, at frequencies higher than 1 Hz, signals probably will not be correlated. In the mentioned studies (e.i. Viens et al., 2015), the ANIRF was used to simulate long-period ground motion (<0.2 Hz) and for such low frequencies, the method seems suitable.

4.4 Invasive methods

Direct sampling of the soil can provide valuable information about soil geotechnical and geophysical properties that can be then used as input in numerical modelling or for verification of existing models. However, the main limitation is a sampling bias and non-representativeness of average site properties. Particularly essential is the possibility of the estimation of shear wave velocity profile in boreholes using active seismic methods. In addition, borehole seismic stations can be employed for empirical reference methods (e.g. SSR) (Steidl et al., 1996) and as vertical arrays in analysis of non-linear soil behaviour (e.g. Roten et al., 2013).

Unfortunately, in an urban environment, the drilling is hindered among others due to the high density of infrastructure, possible disturbances for population, etc. The cost of direct measurements is also significant and it is increasing significantly with exploration depth. That is why; deep boreholes for site response studies, especially in urban areas are rare. However, drilling for geotechnical purposes is common during for example construction works, therefore, some direct geological and geotechnical information can be obtained from local authorities and companies. While gathering the available geological data for the city of Lucerne, we were able

to obtain data from shallow boreholes for several sites thanks to the cooperation with the local government (subchapter 5.1).

For shallow investigation, the relatively cheap SPT (standard penetration test) and CPT (cone penetration test) are commonly used, also in cities. They can be relatively easily implemented in an urban environment, providing estimates of the geophysical and geotechnical properties of the soil. However, their depth range is relatively low (usually up to 30m). The CPT is more sophisticated and provides more information. During the experiment, the probe is pushed vertically into the ground at a standard rate while measuring tip resistance, sleeve friction, and pore pressure (Liao et al., 2002; Robertson, 2009). In the case of the seismic piezocone penetration test (SCPTu), the downhole shear wave velocity is also recorded (Liao et al., 2002). The CPT readings can be used to determine the soil type and its strength properties (Liao et al., 2002; Robertson, 2009). Another important application is the possibility to evaluate liquefaction potential (Robertson and Wride, 1998).

In the next step of site response analysis for the city of Lucerne, we plan also to study non-linear soil behaviour, and to do so, we will take advantage of CPT measurements performed in the area to infer the geotechnical properties (Roten, 2014). The details are to be found in the second deliverable that will be published in 2022. Moreover, a seismic CPT measurement (Attachment 1) was performed close to the station SLUW in Lucerne city center in 2012 and the data will be used while building a 3D model for the area.

4.5 Inversion

The surface wave dispersion characteristics inferred for instance using ambient vibration arrays and MASW technique can be inverted to obtain velocity profiles and then derive 1D, 2D, and 3D models of the area. Combined inversion of the passive array and active seismic dispersion curves help to resolve better the shallow part of the soil structure. However, inversion of the dispersion curves is non-unique and non-linear, that is why additional constraints and good model parametrization are crucial. Joint inversion of the Rayleigh wave ellipticity curve and dispersion characteristics can reduce the variability of the models (Fäh et al., 2003). In the dinver code from the Geopsy package (Wathelet et al., 2004) the modified neighbourhood algorithm (Wathelet, 2008) is used. Both Rayleigh and Love dispersion curves and ellipticity are considered. Several other approaches to such joint inversion were proposed (e.g. Arai, 2005; Picozzi et al., 2005). By adopting additional constraints, it is also possible to retrieve the shear-wave velocity profile by inverting ellipticity or H/V curve (e.g. Arai & Tokimatsu, 2004; Fäh et al., 2003; García-Jerez et al., 2016). Another approach by Sánchez-Sesma et al., (2011) allows inverting H/V spectral energy ratios.

A two-step inversion procedure to constrain bedrock depth was presented by Poggi et al., (2012a). Firstly, the generic velocity profile is derived from the surface wave dispersion characteristics. Then this profile is combined with the characteristics of single station H/V ratios to improve the resolution of the bedrock depth. That procedure was applied in the city of Lucerne (Poggi et al., 2012a). We are planning to repeat it, but using more data and covering a bigger region.

Many researchers work to improve and develop new inversion schemes and software, one example of a novel approach is multizonal transdimensional Bayesian inversion by Hallo et al., (2021) which we used to invert the dispersion curves from the city of Lucerne (subchapter

5.5). It is a joint inversion of Rayleigh and Love wave dispersion curves together with the Rayleigh wave ellipticity curve formulated in the Bayesian probabilistic framework. An important feature is that number of layers is also unknown because of parametrization using Voronei nuclei. Model space is sampled by reversible jump Markov chain Monte Carlo algorithm. The novel thing is the possibility of multizonal parameterization if some additional geophysical constraints for a specific depth range are known.

In subchapter 5.5, a reader can find an example of using the Bayesian inversion by Hallo et al., (2021) for the city of Lucerne. We would like to characterize the velocity structure up to the bedrock which depth varies from several meters to about 100-150 meters.

4.6 Site response proxies

Indirect estimation of amplification using Vs30 as a proxy is widespread, however, site response is too complex to be dependent only on one indicator (e.g. Castellaro et al., 2008). For instance, if the soft sediments are thicker than 30m like in the city of Lucerne, the Vs30 value cannot describe fully the site effects. Other popular indicators of site amplification are among other fundamental resonance frequency f_0 or slope. However, using individual proxies separately can only help to predict the site response to a limited extent (Bergamo et al., 2019). Hence, several approaches to predicting the amplification function from a variety of site condition indicators and proxies are developed (e.g. Bergamo et al., 2019, 2020; Boudghene Stambouli et al., 2017; Derras et al., 2017; Panzera et al., 2021). A detailed overview of the state of the arts is provided among others by Bard (2021) and Cultrera et al., (2021). The idea is to relate one dataset containing information about site condition indicators and proxies with information regarding amplification functions for the sites and then predict the amplification for sites with no direct information about amplification.

In the approach developed by Panzera et al., (2021), empirical amplification function (Edwards et al., 2013) for stations of SED are correlated with the HVRS of ambient vibrations together with the geophysical and geotechnical parameters of the site (Vs30 and thickness of the ice during Last Glacial Maximum) employing canonical correlation. The study shows that empirical amplification functions can be successfully predicted using that approach. The work to apply that approach in the Lucerne area is ongoing. In the coming weeks, we will apply the canonical correlation method (Panzera et al., 2021) in order to estimate the amplification directly from the H/V spectral ratios. Firstly, we will test the technique on the stations of the temporary monitoring network for which the EAF are known, and then we will increase the dataset by adding short single-station recordings.

The connection between several site conditions indicators and proxies and empirical amplification function were also analysed in studies by Bergamo et al., (2019, 2020), firstly using a systematic set of regressions of each proxy separately showing that the best correlations were obtained using frequency-dependent quarter-wavelength (QWL) velocity, Vs30, bedrock depth, and f0. In the next step, the neural network (NN) was employed to predict the amplification functions for stations in Switzerland and Japan from a variety of proxies demonstrating promising results.

Approaches based on the site condition indicators seem to be well suited to an urban area, especially, because many different data that may be used as a proxy is usually available for

cities. However, large uncertainties are involved in predicted amplification, especially in the complex areas where 2D and 3D site effects and non-linear site response are involved.

4.7 Numerical modelling

At this moment, we are still working to build a subsurface model for Lucerne and no numerical methods were applied there. Hence, I will not provide any advice or guidelines based on my experience. However, I will present an overview of the methods used by different authors.

4.7.1 Seismic amplification modelling

Numerical methods can be applied to estimate the amplification using information about the local geological condition, mainly the S-wave velocity profile. For simple 1D structures, analytical solutions exist, a theoretical elastic SH-wave transfer function (SHTF) may be computed with different techniques (e.g. Fäh et al., 2003; Michel et al., 2013; Poggi et al., 2012a) using shear wave velocity profile as an input. The local site amplification functions from the 1D SH-wave modelling can be compared to each other after correcting for the common regional rock reference (Edwards et al., 2013). One of the alternative solutions is based on the quarter-wavelength averaging method (Poggi et al., 2012b). Such 1D approaches are often applied as a part of the site characterization procedure. The surface wave dispersions curves are obtained using for instance passive array measurements, and then they are inverted for shear wave velocity profiles that in turn are used as an input in analytical modeling. We plan to perform such analysis for several sites in the Lucerne area

More complex numerical techniques are needed to simulate 2D and 3D structures. A summary of different methods for predicting and modelling the earthquake ground-motion is provided in Douglas & Aochi, (2008). A detailed overview of numerical methods (e.g. finite-difference, finite-element, finite-volume, spectral-element, boundary element, and discontinuous Galerkin methods) for modelling wave propagation and earthquake ground-motion can be found among others in Moczo et al., (2021) and Semblat (2011). The different levels of complexity can be reached while simulating wave propagation. The elements that need to be defined and can significantly increase the complexity are a type of ground motion excitation (e.g. vertically incident pane wave, random sources, rupturing faults), material properties and constitutive model (e.g. elastic, viscoelastic, anisotropic, single-phase fluid) and geometry of the model.

In recent years, 3D physics-based simulations (PBS) for predicting earthquake ground motion increasingly gain popularity (e.g. Antonietti et al., 2021; Bradley, 2015; Chaljub et al., 2021; Paolucci et al., 2021). Such simulations often include both the modelling of fault rupture and wave propagation. However, estimating earthquake ground-motion using numerical simulations in a wide frequency band is limited, usually, only the low period range is accurately predicted, hence the popularity of hybrid techniques where low and high period ranges are modelled separately (e.g. Liu et al., 2006; Paolucci et al., 2021; Seyhan et al., 2013; van Ede et al., 2020). In addition, to simulate the ground motion realistically, small-scale heterogeneity needs to be represented in a structural model which is often simulated using random fields (e.g. Imperatori et al., 2020; Y. Liu et al., 2019; Pitarka & Mellors, 2021).

Numerical methods can be used also to validate 3D geophysical models of sedimentary basins In the study concerning the Visp area in Switzerland (Alber, 2020), synthetic spectral ratios were generated for the basin using a numerical approach based on random distribution of

seismic source and compared with measured data allowing to assess and improve the accuracy of the 3D model. Similar validation is planned to be performed in the Lucerne area.

4.7.2 Non-linear soil behaviour modelling

For strong motion, soil behaviour cannot be fully explained using the linear response, we need to consider non-linear behaviour. It is a common practice to account for non-linear effects using an equivalent-linear model requiring only a few parameters, however, a fully non-linear wave propagation modelling needs to be applied if complex soil behaviour at larger strain levels is of interest (Bonilla et al., 2005). Non-linear soil response analysis is one of the ongoing topics among engineering seismologists, different methods and approaches have been developed (e.g. Yoshida & Iai, 1998; Yu et al., 1993). A detailed overview of publications in the field of non-linear site response analysis is provided by Regnier (2021). Moreover, the second deliverable that will be published in 2022 will contain a deeper insight into the topic.

In this project, we will mainly use the NOAH by Bonilla (2001) which is a finite-difference code allowing to simulate the non-linear wave propagation due to vertically incident SH wave. It considers the inelasticity and the hysteretic behaviour of stress-strain relation as well as describes the development of the pore pressure under cyclic loading. The model may incorporate the dilatancy and cyclic mobility of cohesionless soils (Iai et al., 1990). The detailed description of NOAH and examples of the program applications can be found among others in Bonilla et al., (2005), Bonilla, (2001), Roten et al., (2014), and (2009). The non-linear calculation using NOAH requires defining several soil properties (Bonilla, 2001) which can be inferred using field measurements, laboratory testing, or estimated with empirical relations. If the dilatant nature of sands is also considered, the model needs five additional dilatancy parameters to be determined (Bonilla, 2001). They can be derived from the triaxial test, CPT, or strong-motion vertical array records (Roten, 2014; Roten et al., 2014). To calibrate dilatancy parameters using CPT data (Roten, 2014), the liquefaction resistance curve is generated from the CPT data employing empirical relations (Robertson and Wride, 1998). Then, the set of dilatancy parameters that explain data the best is found using the inversion scheme with the Neighbourhood algorithm.

5. A site response study in the city of Lucerne

In the following, a workflow for the assessment of site response in an urban area is given for the area of Lucerne. One of our main goals is an evaluation of site response variability across the city and a better understanding of the influence of local geological structures. I will present some of the work performed in Lucerne so far highlighting the challenges.

5.1 Data mining

The typical first step during the site response study is a compilation of geological and geophysical data available for the area. Because of geological conditions, historical earthquakes, and first of all, because of the concentration of exposed elements, Lucerne was subjected to a few studies concerning seismic hazard assessment and site characterization, allowing us to better plan our further investigations. Poggi et al., (2012a) investigated local seismic site response in the city centre, combining single station and array ambient noise recordings. As a result, they improved the resolution of basin geometry and estimated a

simplified amplification model. Several permanent broadband accelerometers including one borehole station belonging to the Swiss Strong Motion Network (SSMNet) (Hobiger et al., 2021; Michel et al., 2014) are situated in Lucerne city centre and around Lucerne Lake (Figure 9). Standard site characterization procedures have been performed to infer the local site conditions for most SSMNet stations, providing us with detailed information about fundamental frequency, shear velocity, and geological structure at some selected sites in Lucerne (Hobiger et al., 2017; Michel et al., 2013; Poggi et al., 2013b). We also established a collaboration with cantonal authorities and private companies, which provide us with additional information (e.g. CPT data, some geotechnical investigation reports, reports from drilling). The list and map of some available data can be found in Attachment 1, location of previous ambient noise vibration measurements is shown in Figure 11.

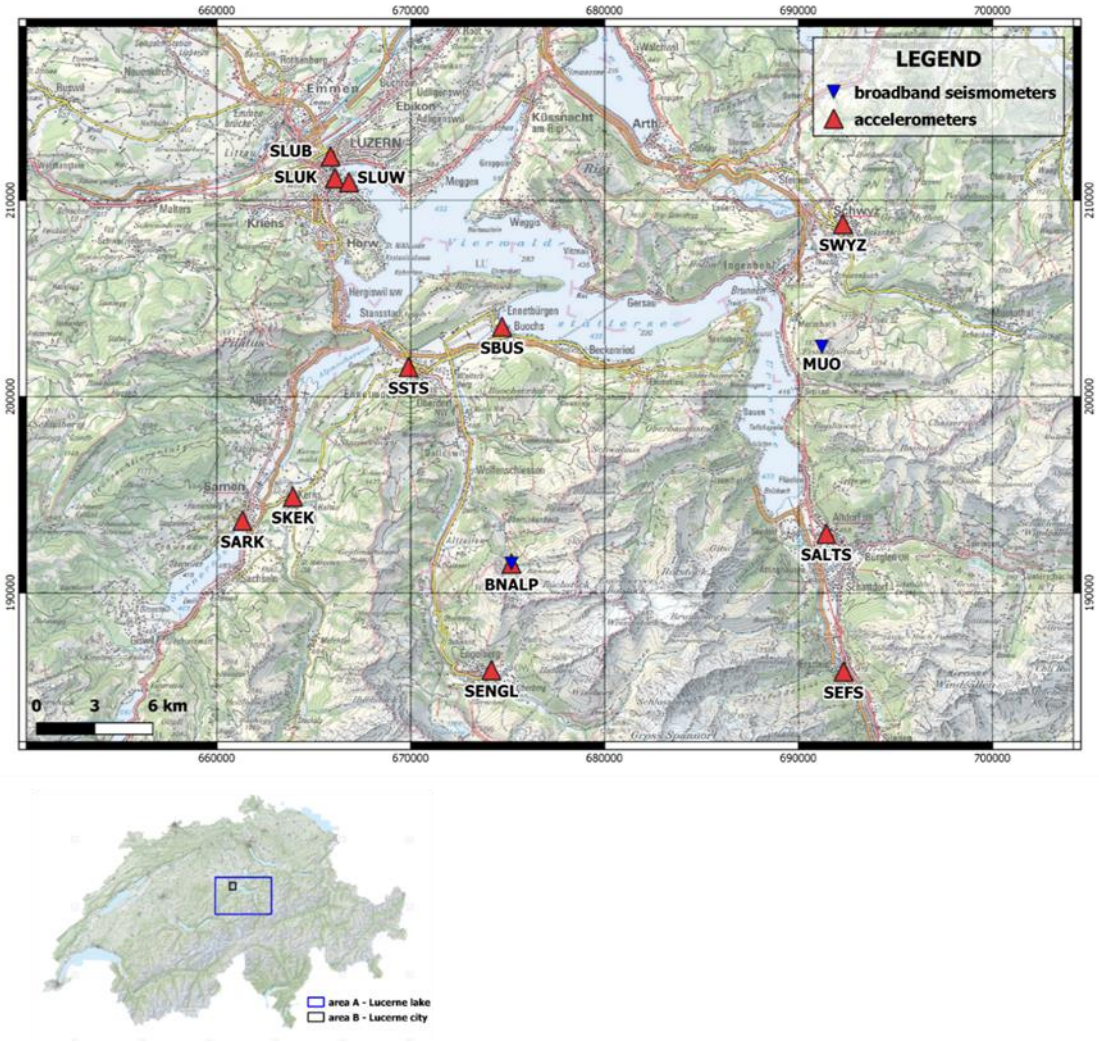

Figure 9. The map shows the permanent seismic stations located around Lucerne Lake. Three stations (SLUB, SLUK, and SLUW) are in Lucerne city center. SBUS is a borehole station. The area showed on the bigger map corresponds to the blue rectangle on the map of Switzerland. Base maps source: Federal Office of Topography Swisstopo, (2021)

One of the few advantages of working in an urban environment is the relative easiness to find a variety of data. Cities are always a focus of interest, concentrating funding for different research and investigations. For our purposes, all kinds of information, not only directly related

to engineering seismology, may be useful, including particularly geotechnical or hydrological investigations. However, in order to access most of such information or facilitate obtaining permissions for measurements, collaboration with local authorities is essential. From my experience, it is one of the most important steps during planning the site response investigation in an urban environment.

5.2 Empirical methods

5.2.1 Installation of temporary local seismic monitoring network

We have decided to install a temporary seismic monitoring network in the studied area to record weak ground motions from low-magnitude or distant earthquakes, that can be used then to estimate the variability of site response. Moreover, the long-term ambient noise recordings can be used for the analysis of the spatial and temporal distribution of the ambient noise wavefield in the area.

After a virtual and personal inspection of many sites in Lucerne and neighbouring areas, we found several places characterized by different geological and geotechnical conditions suitable for installation (Figure 11). One of the important factors affecting the choice of the site was the possibility to connect the instrument to electrical power and safety (the place should be protected by some enclosure and not open to the public). We targeted especially sites important for the society, like schools and hospitals, not only due to the elevated risk but also because it is easier to get permission for setting up the seismic station there. We tried to find free-field sites, far from high buildings or underground structures and away from strong transient sources (e.g. highway, railway); however, it was not always possible in the densely populated urban environment.

Figure 10. Example of the installed seismic station of the temporary network. More information in the text. Photo: Paulina Janusz

Nine short-period seismometers Lennartz 5 seconds (LE-3D 5-s) with 6-channel Centaur digitizers were installed in November 2019. The sensors were buried 0.4 m below the ground, except for one, which was situated in the underground parking – the instrument was laid directly on the concrete floor. All sensors were aligned to the magnetic north and situated

horizontally to the surface. The digitizer, extra battery, and cables were protected using a waterproof cover. A small fence secured the whole installation (Figure 10). Real-time communication was ensured. The stations were dismantled in May and June 2020. In December 2020, we installed again a temporary seismic local monitoring network, adding two more stations. Attachment 2 summarizes the most important information concerning the network and shows some geological and geotechnical characteristics of the sites. To supplement the dataset, we also utilize recordings from three permanent accelerometers located in the Lucerne city center belonging to the Swiss Strong Motion Network – SSMNet (Hobiger et al., 2021; Michel et al., 2014).

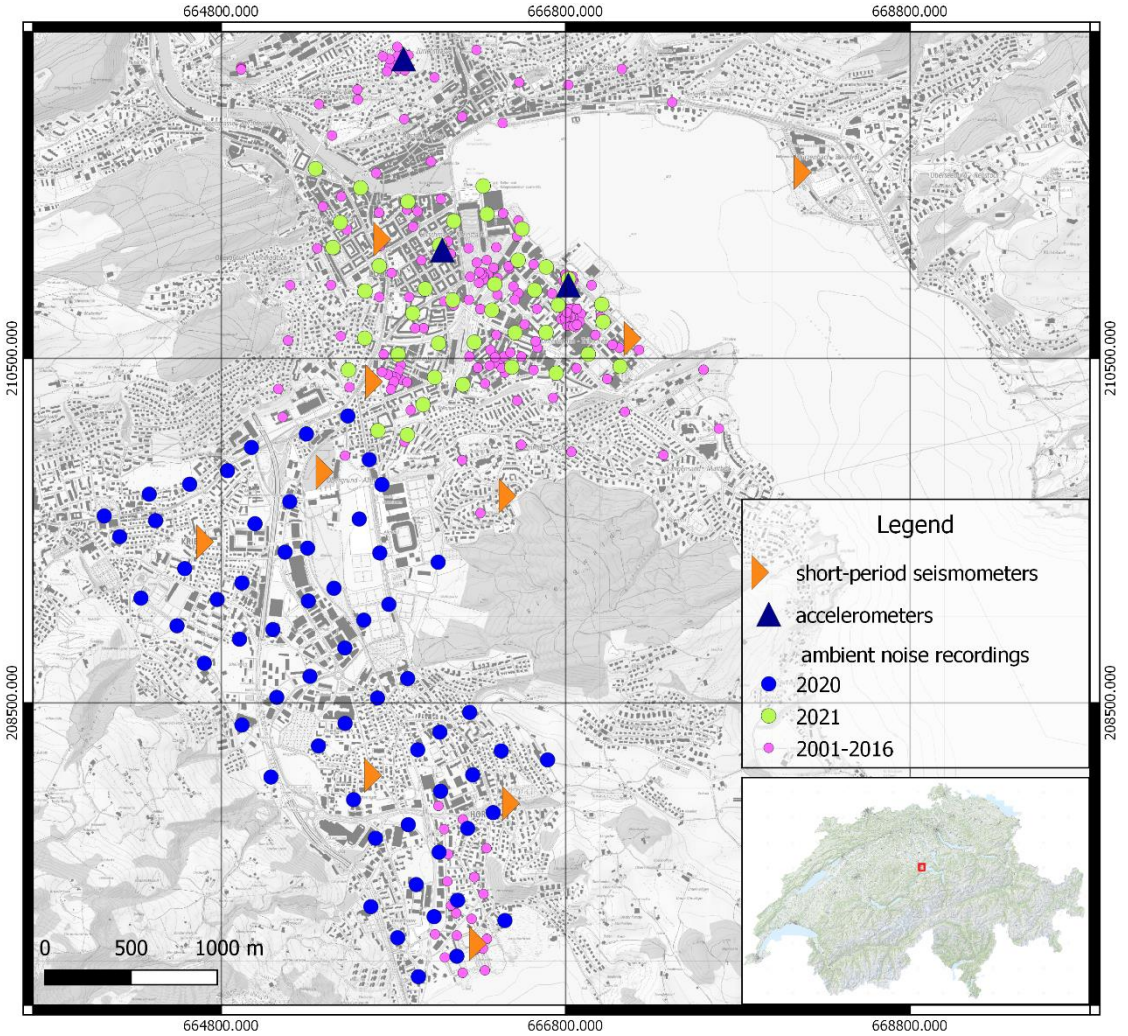

Figure 11. Seismic stations in the Lucerne area and ambient noise measurements. Short-period seismometers are part of the temporary local network, while accelerometers belong to SSMNet. Red rectangular on Switzerland map shows the location of the investigated area. Base maps source: Federal Office of Topography Swisstopo, (2021).

5.2.2 Processing

While our temporary network was recording, we were able to record a number of local (Figure 12) and teleseismic earthquakes (Attachment 3). For each site, all recordings were first processed using the ObsPy library (Beyreuther et al., 2010) applying instrumental correction and bandpass filter (a cosine taper with corner frequencies: 0.01, 0.05, 95, and 100 Hz). For

further analysis, we considered part of the signal from the P-wave until the coda wave arrival (Perron et al., 2018b). The signals were analysed in the frequency domain - the Fast Fourier Transform function from Matlab was used. The required signal-to-noise ratio in our analysis is equal to three (Figure 13). To decrease the effect of transient anthropogenic sources, I calculated the statistics of several 30s noise windows to estimate the level of background noise. The part of the signal was taken for further analysis only when the signal-to-noise ratio is above the required threshold for more than half an octave. The SSRs were computed only for those basin-rock station pairs for which the distance between stations is at least 5 times smaller than the approximated epicentral distance for a given event. The smoothing was performed using the Konno & Ohmachi, (1998) filter with a b-value of 40. The final SSR function is a geometrical average over the population of events. The horizontal component H is defined as follows:

$$H = \sqrt{E^2 + N^2}$$

where E and N are subsequently eastern and northern components.

Moreover, for each station of the Swiss monitoring network, if the signal-to-noise ratio is more than 5 in a broad frequency range, the empirical amplification functions (EAF) (Edwards et al., 2013) are computed automatically for each local earthquake.

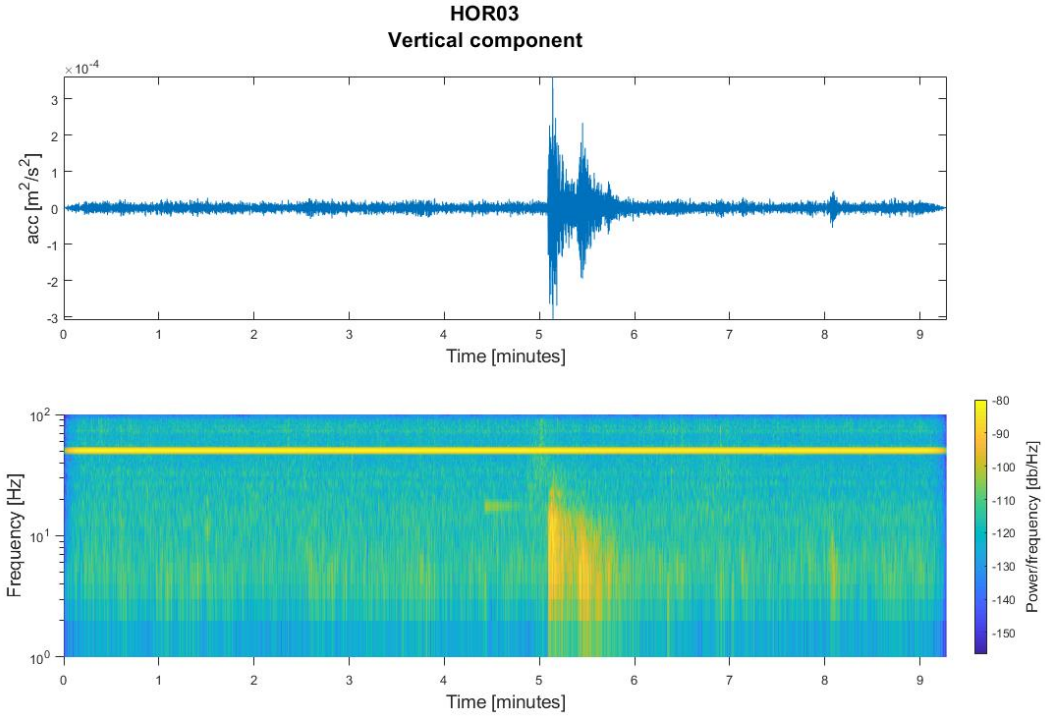

Figure 12. An example of an earthquake recorded by station HOR03 (event on 2019-11-30 02:14 in Verbier VS with a magnitude 3.0). The lower plot is a spectrogram using a short-time Fourier transform. The time on the lower axis is counted from the beginning of the recording.

5.2.3 Results and discussion

SSR method

Amplification functions relative to the rock station LUZ01 derived using the SSR method are plotted in Figure 14a for each temporary and permanent station. All figures have the same scale. As a background, we use the map of the thickness of unconsolidated deposits derived from the bedrock elevation model issued by the Swiss Federal Office of Topography to show the consistency with geological data. Two stations with a flat spectral ratio (SLUB and HOR01) are also rock stations. For stations situated in the deeper part of the basin, the peak amplification reaches or exceeds 10 at about 1-1.2 Hz. In general, the consistency with the thickness of the unconsolidated deposits map is observed: the thicker the sediments, the higher the amplification and the lower frequency of the peak. For HOR02 and HOR03 that are located in the deepest part of the basin; the amplification peak is at about 1 Hz with an amplitude of about 10. Four stations (LUZ03, SLUK, SLUW, and LUZ02) in the city center are aligned along the basin. A consistent shape of one peak at around 1 Hz and amplitude of 10 and the lower second peak is visible and the reasons may the shallow sediments or 2D site effects. It is worth mentioning that the second peak is not visible for LUZ04 located on the opposite side of the lake. For the KRI01 station is situated at the basin border, the peak frequency for the is 2,5 Hz and amplitude is about 8. For the KRI02, the peak amplification is lower and its frequency higher compared to KRI01, even though it is placed where the bedrock is still relatively deep according to the map of the thickness of the unconsolidated deposits. In addition, the peak is wide with no clear maximum for KRI02. The reason may be the basin-edge generated surface waves or errors of the gravity-derived map of sediment thickness.

Even though, the standard deviation represented by error bars seems to be small (Figure 14b); for some stations, the number of recorded earthquakes that exceed the required signal-to-noise ratio is low because of the high background noise level (Figure 14c). For only two stations, more than 20 events exceeded the required signal-to-noise ratio and only in the limited frequency band. For most of the network, on average 17 high-quality events were recorded, however, that number is much lower for higher and lower frequencies. Nevertheless, the frequency ranges where we observe the peak amplification have the highest number of contributing events, hence the highest amplification values can be treated with relative confidence. Two stations have significantly lower numbers, LUZ05 because it was deployed only in 2021 and LUZ02 due to technical problems in 2020. Therefore, we may need to install the network for a longer time to obtain more certain results and estimate amplification function with sufficient accuracy using empirical methods. Such problems are typical for low seismicity urban areas generating additional costs and increasing workload.

EAF function

We compare the EAF function with the SSR method (Figure 15). Both techniques give comparable results, even though, their reference sites differ: in the SSR method, we use a local rock site and in EAF calculations, the Swiss reference bedrock profile (Poggi et al., 2011). Most of the differences between curves can be explained by lower accuracy because of the lower number of earthquakes considered in the EAF, the standard deviation is also significantly higher. Firstly, only local earthquakes are taken into account in the EAF calculation, for the SSR, teleseismic events contribute and help to better resolve the low-frequency band. Secondly, higher standards for minimum signal-to-noise ratio are adopted for the EAF. Therefore, for the stations characterized by a high level of human-generated noise, only a few

events contribute and for those stations, the difference between the SSR and EAF is the highest. However, even for such sites, the SSR results are inside the confidence limits of the EAF method.

In more sophisticated empirical methods such as the EAF, the number of earthquakes required is even higher than in the SSR method because higher quality of data is needed. Hence, the method is relatively slow for estimating the basin response in the low-seismicity urban areas. However, it provides amplification to a common Swiss reference-rock velocity profile. In our case of low seismicity, only the EAF of the rock outcrops can be estimated with high accuracy if stations can be installed only for several months. By combining with other methods like the SSR or ambient noise techniques, the EAF for rock sites can be used to provide absolute referencing for local basin models.

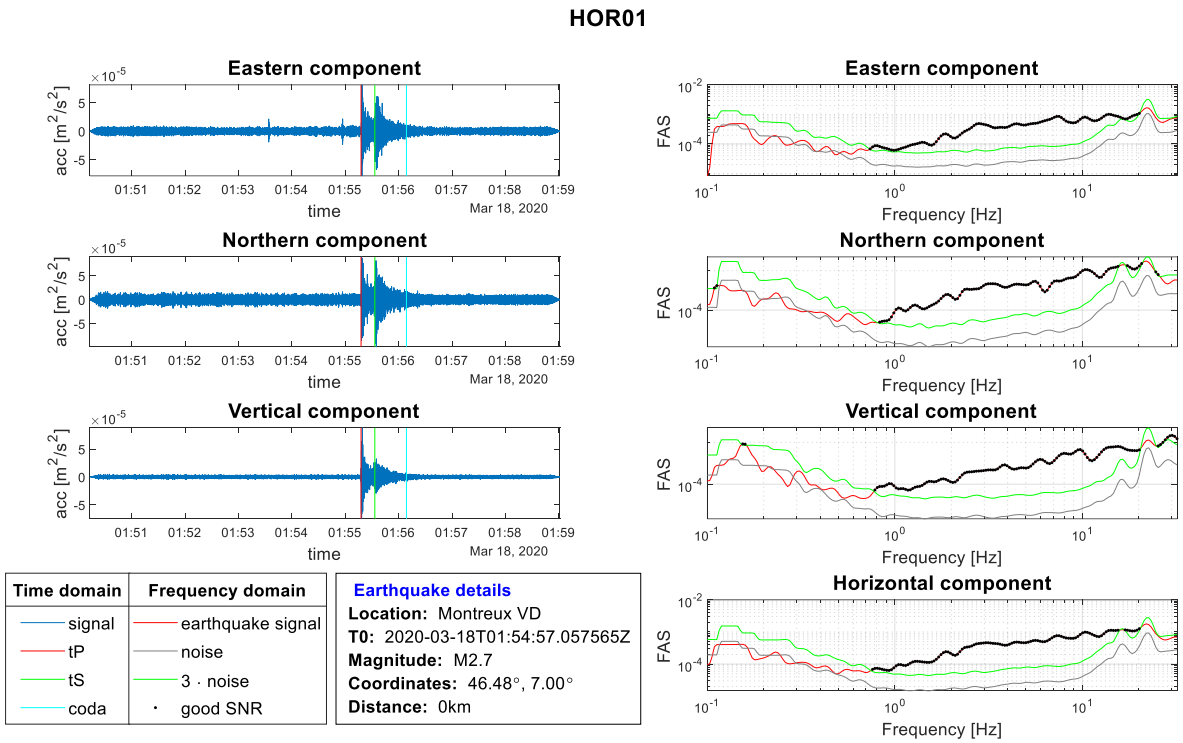

Figure 13. Example of the recorded earthquake in time (left panel) and frequency domain (right). In this study, the earthquake phase from P-wave to the coda wave is considered. On the right panel, the frequency bands where the signal-to-noise ratio is sufficiently high are highlighted using black dots.

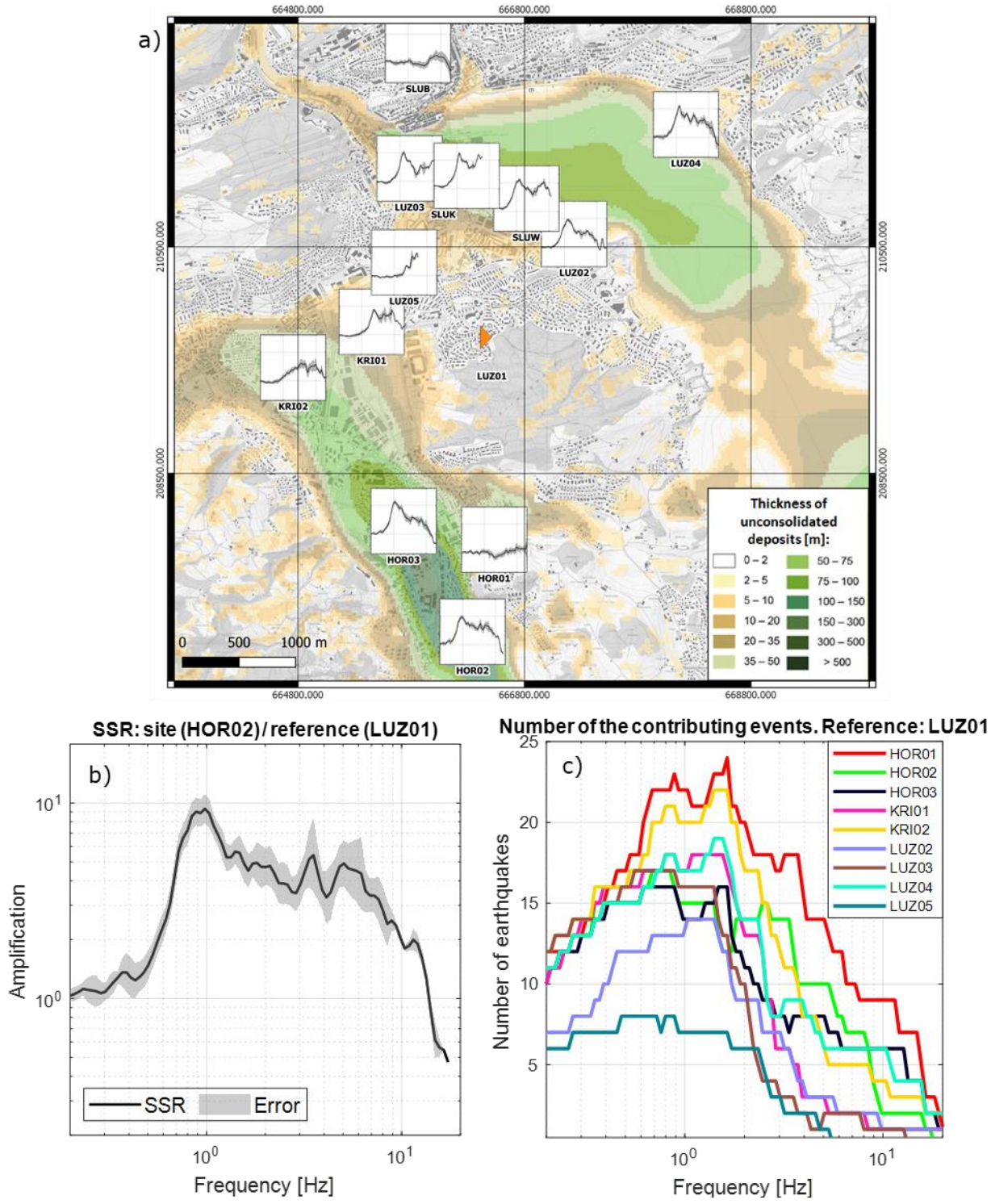

Figure 14. a) The amplification function for stations located in the Lucerne area using the SSR method referenced to rock station LUZ01. In the background, the thickness of the unconsolidated deposits map is shown. Base maps source: Federal Office of Topography Swisstopo, (2021). b) SSR curve for the HOR02 station with standard deviation. c) The number of contributing events for each frequency for all sites.

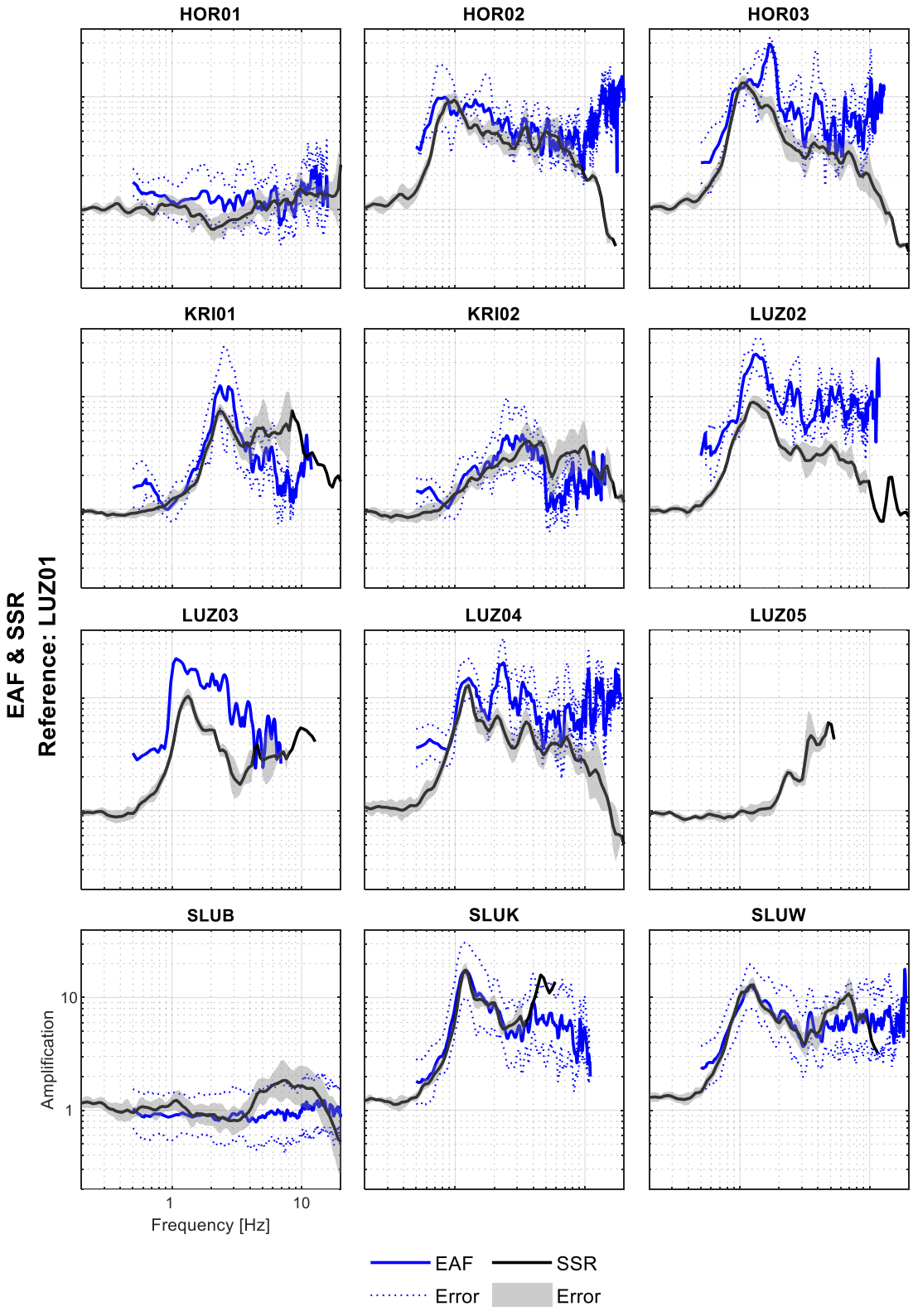

Figure 15. The relative amplification functions with the SSR method (reference – rock station LUZ01) compared to the EAF (reference – Swiss reference bedrock).

5.3 Evaluating site amplification function using ambient vibrations

5.3.1 Single station measurements

In June 2020 and in April 2021, we carried out two surveys both including several dozen of densely distributed single-station noise measurements (Figure 11, Figure 16). Overall, we measured noise at 100 sites leaving instruments (short-period seismometers Lennartz 5 seconds LE-3D 5-s) for a minimum of 1–2 hours. The campaigns were performed when the stations of the temporary network were still operating, enabling us to apply the SSRh method.

Figure 16. Example of measurement of ambient noise close to the Lucerne train station during the survey in April 2021. The setup consists of a Lennartz 5-s sensor and Centaur digitizer. Photo: Paulina Janusz

5.3.2 Processing

SSRn method

For each temporary and permanent station that was described in subchapter 5.2.1, we selected randomly 24h of continuous noise recording. The signal was divided into shorter windows and FAS was calculated using the Matlab spectrogram function. The windows length and overlap value were adaptive depending on the signal length to optimize the computing time. For instance, for 24h recording the window length was 80 s with no overlapping window, while for one hour-long signal, the length of the window was 40 s with 50% overlapping. For each pair of the stations, we calculated spectral ratios, which were then averaged with geometrical mean after the previous removal of outliers. The final curve was smoothed with Konno & Ohmachi, (1998) filter with a b-value of 40. For short ambient noise measurements (subchapter 5.3.1), the same processing was applied but considering the whole recording.

SSRh method

We used previously calculated SSR and SSRn functions to estimate the SSRh for each temporary and permanent station:

$$SSRh_{\frac{site}{rock}} = SSR_{\frac{intermediate}{rock}} \cdot SSRn_{\frac{site}{intermediate}}$$

The intermediate station has to be located in the same basin as the site. To avoid the subjective choice of intermediate site in case a few potential intermediate stations are located close to the considered site, we calculated a weighted geometrical mean of several realisations of the SSRh function computed using different intermediate stations. The weight is an inverse of the squared distance between the intermediate station and site.

We applied the same procedure to the sites where we recorded ambient noise during our two measurements campaigns (subchapter 5.3.1).

5.3.3 Results and discussion

In Figure 17, we can observe that the SSRn approach overestimates the amplification compared with the SSR method. While the general shape and frequency of the peak are comparable, the amplification factors are similar only for the frequency band lower than the frequency of the first peak. Such observations were confirmed in the past by several authors (e.g. Field et al., 1990; Perron et al., 2018a). Instead, the SSRh method seems to predict more reasonable amplification factors and usually agrees with SSR. The differences are more pronounced for shorter periods. Generally, the uncertainty for the SSRn and SSRh are higher than for the SSR, the reason is a high variability of noise wavefield and influence of transient sources.

In , the amplification model for the Lucerne area derived using the SSRh technique is presented, it is referenced to rock station LUZ01. A presented example is for 1.2 Hz; however, we have estimated the site response for several frequencies. Snapshots for different periods show consistency with the information about bedrock depth (Figure 14a). For the deeper part of the basin, the peak amplification is moved to longer periods. Based on the model, we can expect the amplification up to 10 for frequencies between 0.8 and 2 Hz.

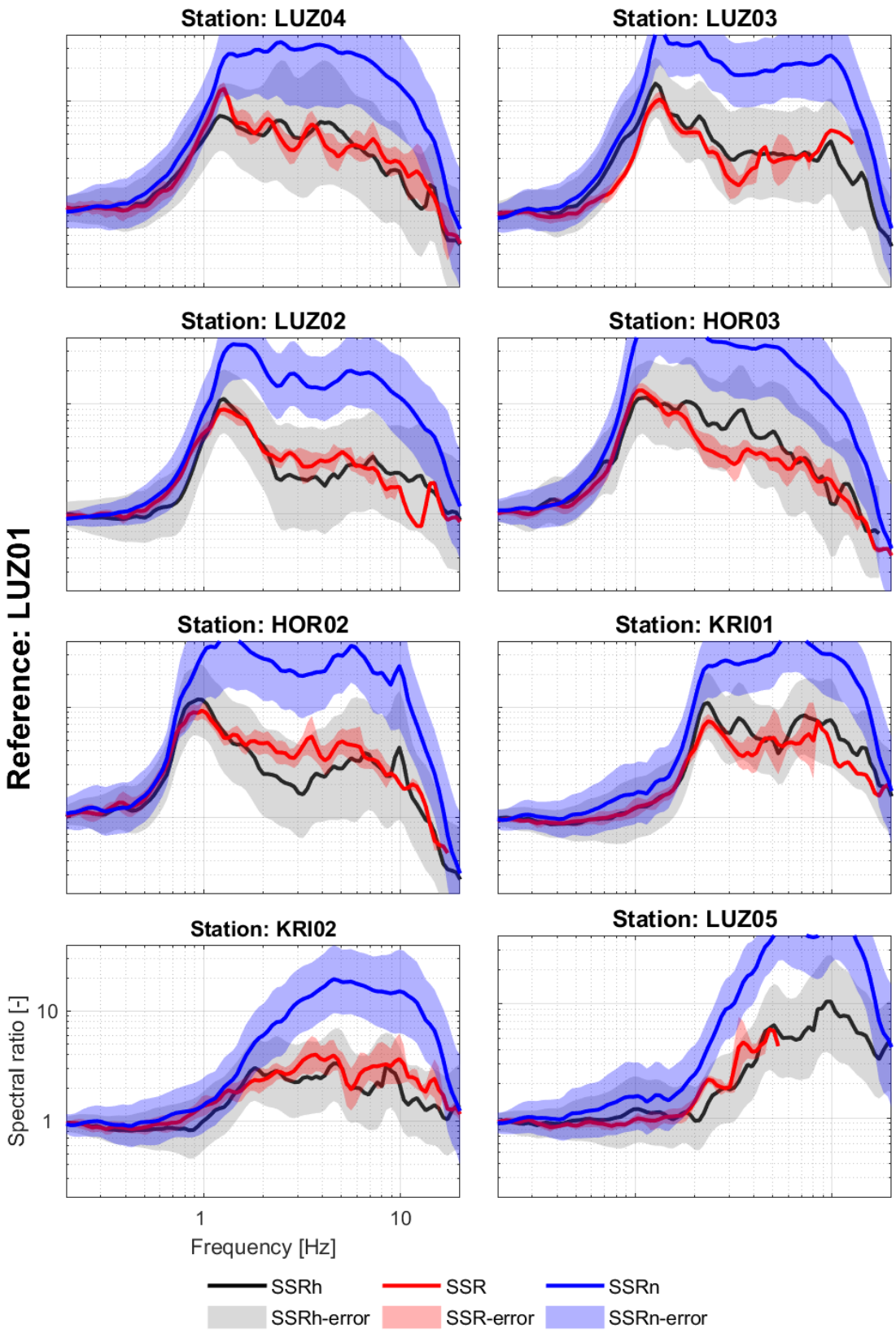

Figure 17. The relative amplification functions using the SSR, SSRn, and SSRh methods (reference – rock station LUZ01.

While the SSRn method does not provide us with correct amplification factors, especially in the urban environment where many strong transient sources can affect the results, the SSRh approach seems to be well suited to cities. The problems of the SSRn method are corrected by using the intermediate reference station inside the basin for the SSRn computation. Ambient noise has the advantage of being easily and quickly recorded everywhere, even in a densely populated city, allowing the creation of a high-resolution map of basin response. The method is relatively cheap; no large monitoring network is needed since only two stations are required, however, a few extra intermediate stations are recommended to ensure good sampling of basin conditions and to verify the validity of the SSRn inside the basin. However, although the obtained results are very promising, more work on verification of the method is needed. Before using the method is also recommended to investigate the influence of time of the day when noise is recorded because for some pair of the stations, the ambient noise wavefield differs during the day and the night due to the intensity of human activities (Janusz et al., 2021b). Based on my experience, I would advise longer recording times for the SSRh method - a few hours or even 24h of recording.

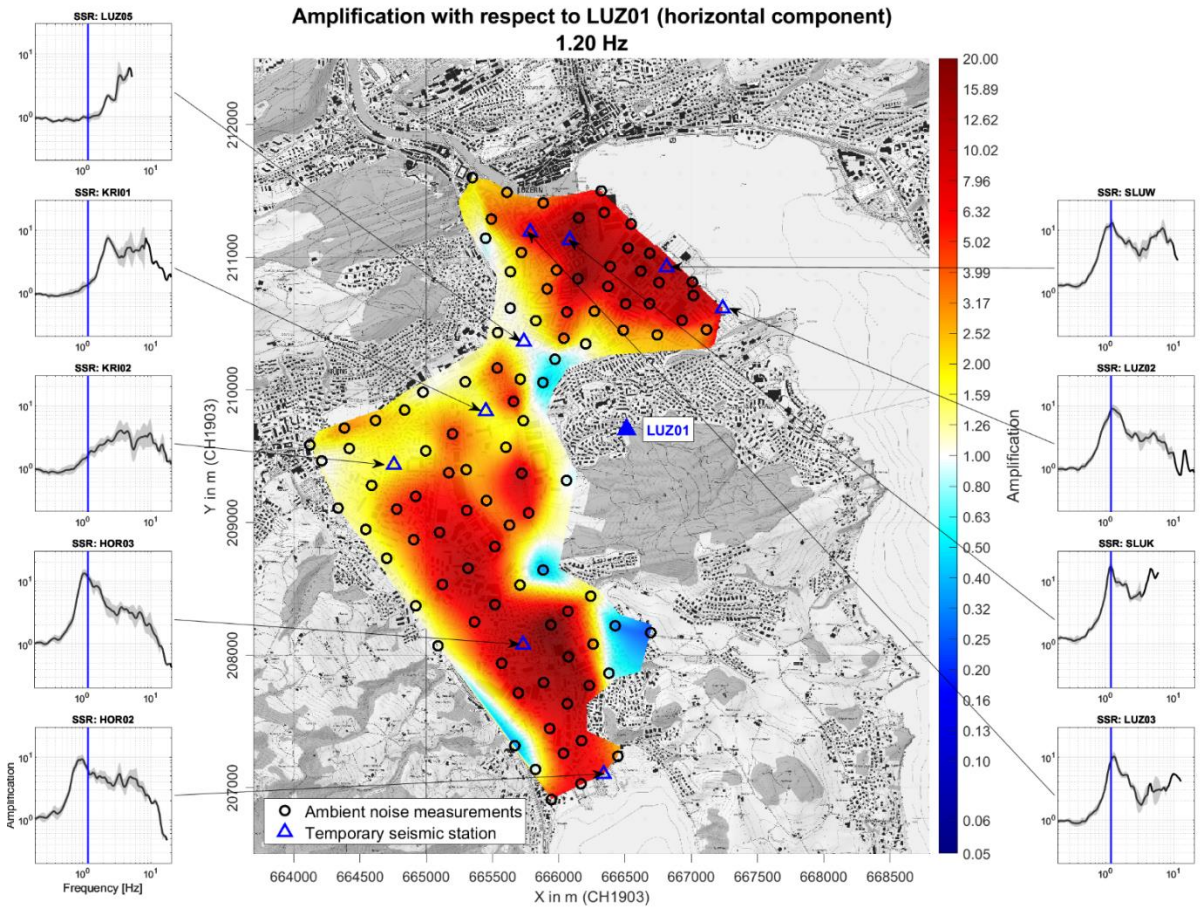

Figure 18. Relative amplification for Lucerne area for 1.2 Hz (reference – rock station LUZ01). Blue triangles are the sites of the temporary monitoring network, the SSR functions for those points are shown outside the map, blue lines show the value for 1.2 Hz. Black circles represent ambient vibration measurements. Base maps source: Federal Office of Topography Swisstopo, (2021).

5.4 Mapping the fundamental frequency of the resonance

5.4.1 Data and processing

In addition to 100 single station measurements performed in Lucerne in 2020 and 2021, we have taken advantage of a few hundred ambient noise recordings carried out in Lucerne since 2001 (e.g. Poggi et al., 2012a) (Figure 11). The data was collected using different instruments and in the case of my measurements, recordings are 1-2h, while old data is shorter (about 0.5-1h). We included also ambient noise recorded at temporary and permanent stations. To reduce computation time and minimize the effect of vibration generated by human activities, the 4h of night uninterrupted noise records were selected from their continuous recordings. For each raw signal, we applied the RayDec analysis (Hobiger et al., 2009) to obtain information about the Rayleigh wave ellipticity curve. Then, I selected manually for each site the fundamental frequency of resonance.

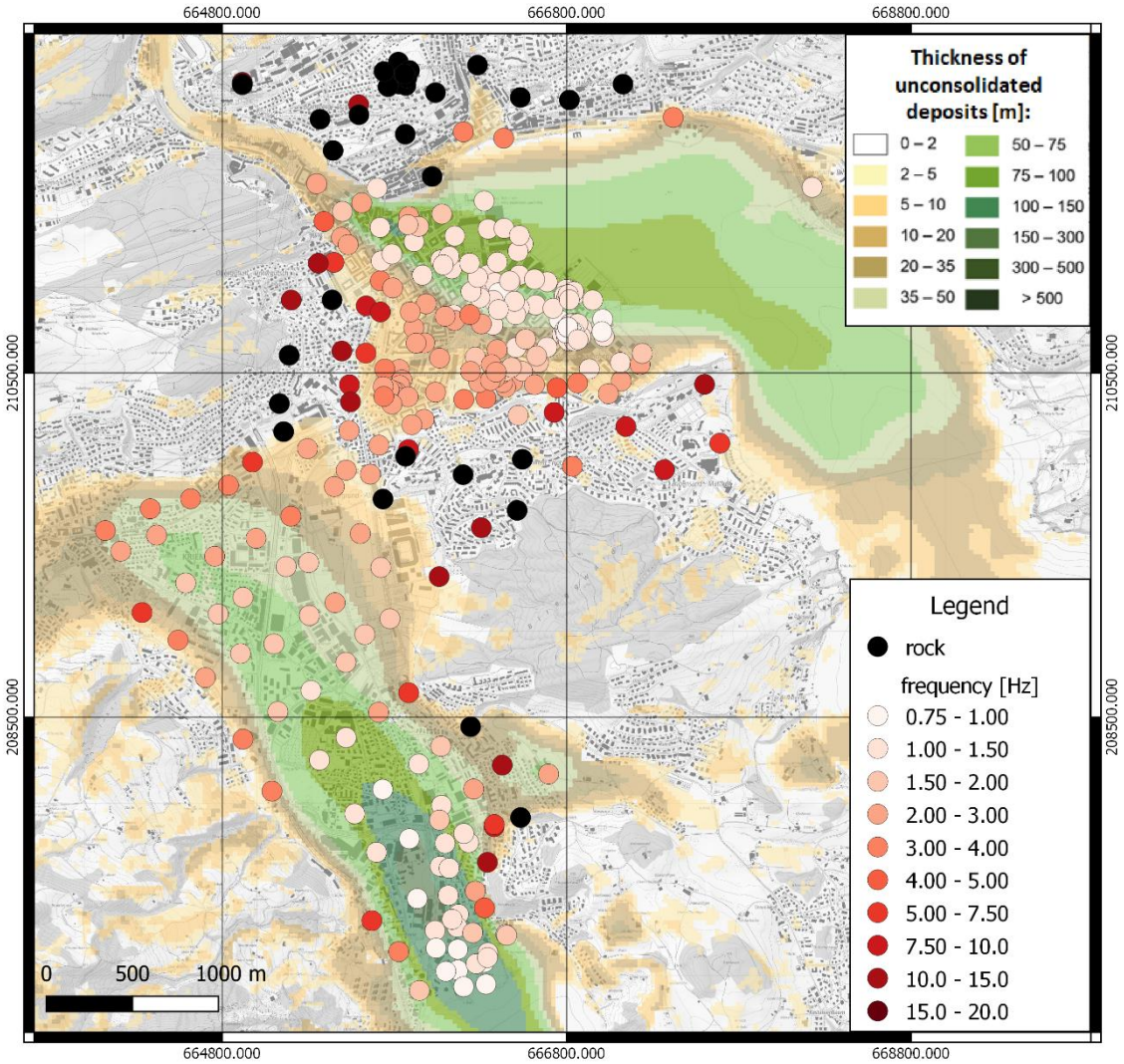

Figure 19. f_0 for each site. The background map is the thickness of the unconsolidated deposits derived from the gravity measurement. Base maps source: Federal Office of Topography Swisstopo, (2021).

5.4.2 Results and discussion

We mapped the frequency of the peak of the Rayleigh wave ellipticity function for the Lucerne basin using more than 300 points (Figure 11). The lighter colors correspond to the lower f0 values. For sites which based on geological information are located on the rock, the peak was often not discernible. When compared with the map of the thickness of unconsolidated deposits, we can observe a good agreement; the lower frequencies correspond to the deeper sediment-bedrock interference. However, our results give more detailed information, especially at the basin borders. Such information can be used to create a better model of bedrock depth in the Lucerne basin.

Fundamental resonance frequency f_0 is often used as site response proxy because it is related to shear wave velocity below the site and the thickness of unconsolidated deposits. However, the amplitude of the H/V curve cannot be used as a direct estimation of the amplification. In Figure 20, the comparison between SSR and HVSR is shown. While the f_0 is similar to the frequency of the amplification function peak, the amplitudes of both curves, especially for frequencies higher than the peak, are different.

Mapping of the fundamental frequency peak is an easy and simple method to get an overview of the investigated area and qualitatively assess the site response that is why it is commonly used, also in an urban environment. Although the high intensity and variability of the ambient vibration wavefield in cities can affect the recordings, from my experience, the H/V ratios appear to be relatively repetitive and providing reliable outcomes, independent of disturbances. However, we need to be careful and critical not to identify a narrow-band industrial peak as the fundamental resonance frequency. This analysis can be supported by reducing the smoothing of H/V spectral ratios or by the analysis of unsmoothed power spectra of the three components of motion (e.g. Bard et al., 2008).

5.5 Ambient vibration array reprocessing

In the next step, we will look deeper into the processing of the passive array that allows obtaining surface waves dispersion characteristics of the subsurface.

5.5.1.1 Data

In 2007, five ambient vibration array measurements were performed in Lucerne city center (Poggi et al., 2012a). Their location is shown in the map (Figure 21) and recording time and date of measurement in Table 1. The measurements were conducted using short-period seismometers Lennartz 5 seconds (LE-3D 5-s) with a 24-bit data logger (Quanterra Q330). Array SBB and Array 1 consisted of two concentric rings: smaller and bigger, while a cross-shape deployment forced by the road network was used for Arrays 2, 3, and 4. Such configuration is often used in an urban environment. Array 1-4 were recorded during the day and are generally noisy and of very low quality, not only because of the high level of cultural noise but also because of short recording time. Array SBB was deployed in the middle of the main train station, however during the night time. All trains were stopped for 2 hours in order to minimize the disturbances and to ensure the high quality of the data.

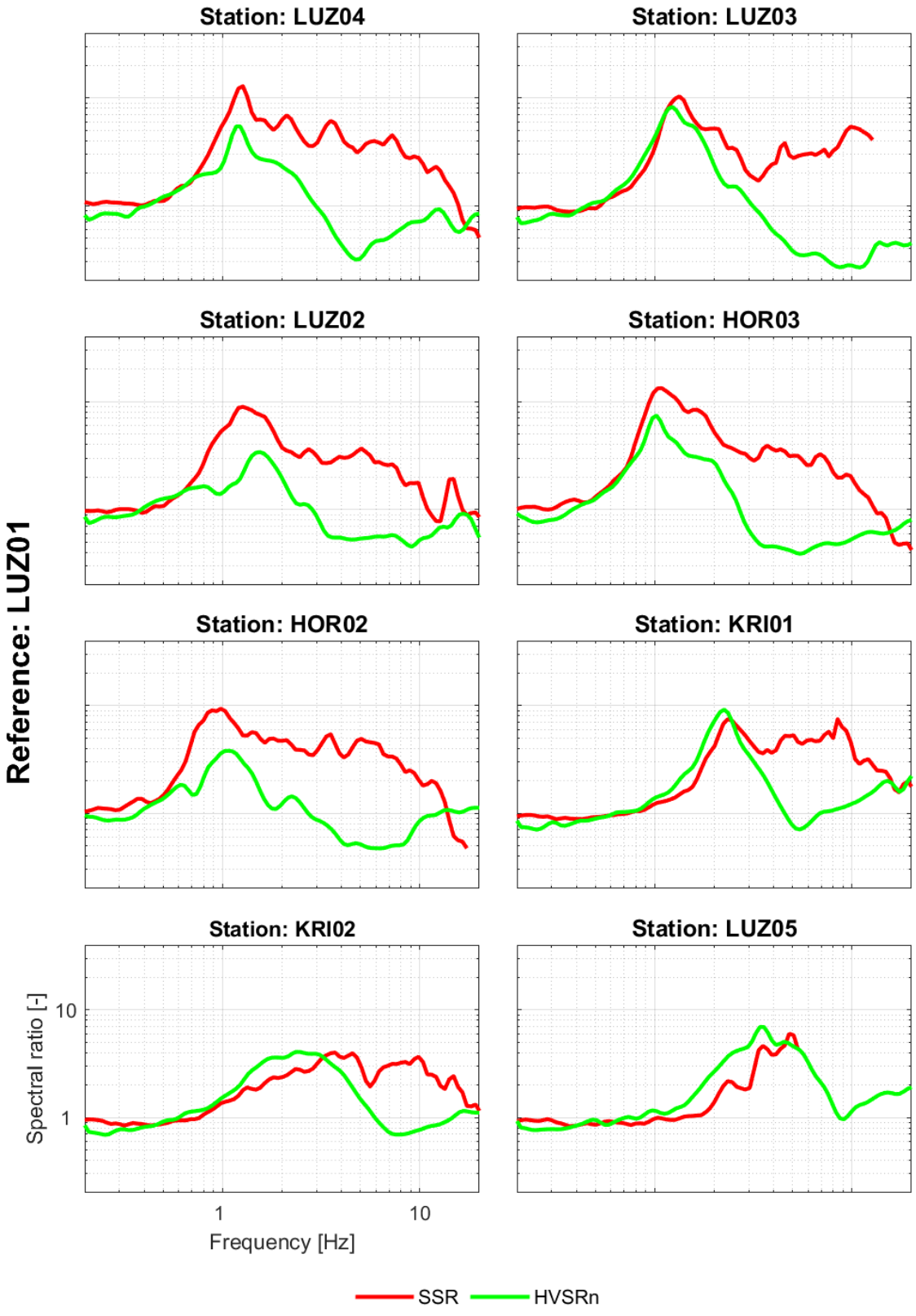

Figure 20. The relative amplification functions using the SSR method (reference – rock station LUZ01) and Rayleigh wave ellipticity curve using the RayDec method (Hobiger et al., 2009).

Figure 21. Location of ambient vibration array measurements performed in Lucerne city center in 2007 (Stamm et al., 2008).

Table 1. Some details about ambient vibration arrays performed in Lucerne city center in 2007 (Stamm et al., 2008). The location is shown in Figure 21.

Array	Ring	Date	Start time	End time
Array 1	Small	13.06.2007	08:30	09:00
	Big	13.06.2007	10:30	11:30
Array SBB	Big	15.06.2007	00:00	01:00
	Small	15.06.2007	01:55	02:18
Array 2		13.06.2007	13:25	13:45
Array 4		14.06.2007	12:50	12:50
Array 3	not in database			

5.5.1.2 Processing and examples of the results

In 2007, the data was processed using the three-component high resolution f-k method (Poggi et al., 2012a; Poggi & Fäh, 2010). Then, the dispersion characteristics were inverted to infer shear wave velocity structure but only for Array SBB. That is why we have decided to reprocess all arrays from 2007 using also different methods, which did not exist in 2007 in an attempt to retrieve some new information about subsoil structure in the investigated area. I will present step by step the procedure illustrating it using examples from the reprocessed arrays. The stages described below are a part of the standard processing procedure used for site characterization in the SED Engineering Seismology group.

Array resolution limit determination

The warangps from the Geopsy package (Wathelet et al., 2020) is used to calculate the theoretical resolution limits of an array from the coordinates of the deployment. In Figure 22a, we see the array transfer functions on the left side and in the right - resolution limits depicted as curves on the slowness-frequency plot. They define the minimum and maximum wavelength that should be used for the inversion of dispersion curves.

Rotation of the components to a common north

In the field, it is common to use a compass to align the sensors to magnetic north. However, human errors can be significant and sensor misorientation of about 10° or more are common. In addition, there is an abundance of ferromagnetic materials or interfering electromagnetic fields in urban areas that can disturb the compass readings. An example is Array SBB located inside the train station where serious errors in orienting stations emerged (Poggi et al., 2012a) due to tracks, traction wire, wagons, etc.

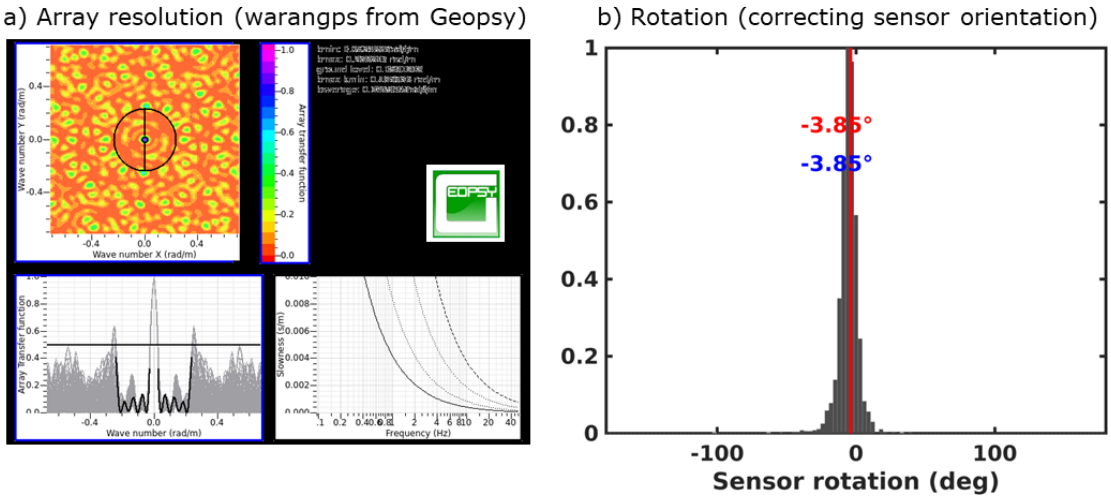

Figure 22. a) Theoretical array resolution using warangps from the Geopsy package. b) Example of histogram of sensor's misorientation.

While quality control of the stations' alignment is always needed, it is a particularly significant problem in urban areas. To correct the orientation of the sensors, one reference station has to be chosen for which ideal alignment to magnetic north can be assumed. The algorithm then utilizes a low-frequency range of ambient noise to correlate horizontal signals of all stations to the reference. Figure 22b shows a histogram of all rotation angles maximizing the correlation.

The best value marked with a red line is then used to rotate the horizontal component. The procedure is repeated for all stations.

Horizontal-to-vertical ratios

For each deployment, the H/V curve is calculated using different methods e.g. classical (Nakamura, 1989), time-frequency analysis (Poggi et al., 2012a), RayDec (Hobiger et al., 2009). By putting together curves for each array sensor, we can check for possible variability of soil structure below the array and assess if an area where the array was deployed is 1D. An example for the smaller ring of Array 1 indicates a very homogenous site, while for Array 2; some variability is visible (Figure 23).

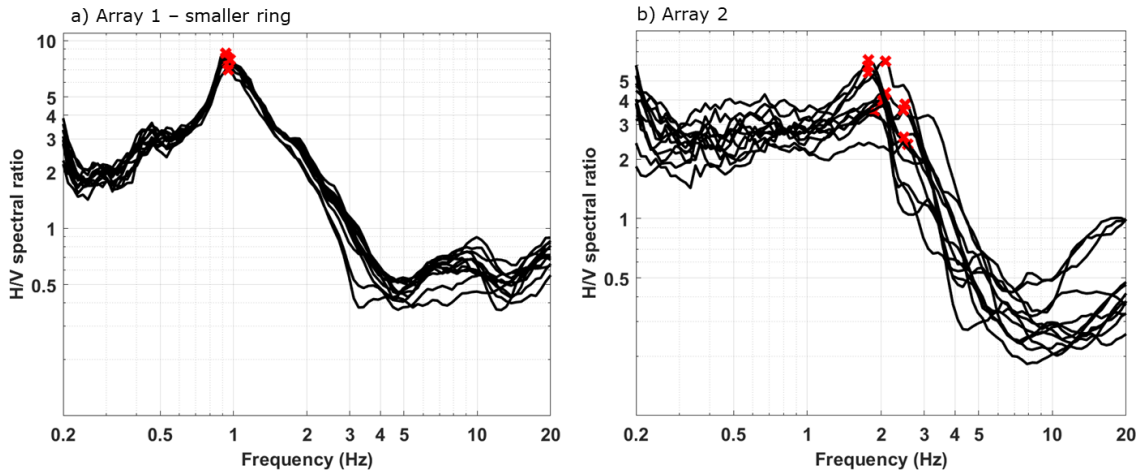

Figure 23. H/V using time-frequency analysis for each array deployment.

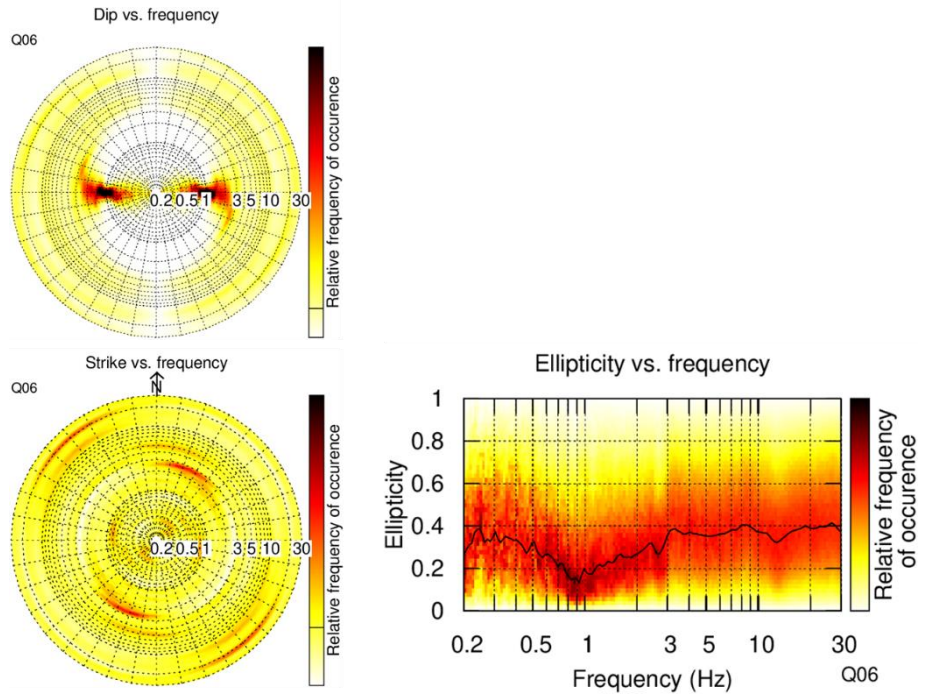

Figure 24. Polarization analysis for a station of Array 1.

Polarization analysis

The polarization analysis of Burjánek et al., (2010) allows checking for any directional effects (2D or 3D resonance), which is especially important in sites located in the sedimentary basins. In Figure 24, the results of polarization analysis for one of the stations of Array 1 are shown. Two polar plots are respectively the dip and strike of the particle motion ellipse. The dip is defined as an inclination from the horizontal plane, while the strike is azimuth in the horizontal half-plane. If at some frequency, we see clearly that one direction is preferred, it means that the wavefield is polarized in this direction. The last graph shows the ellipticity of particle motion as a function of frequency. If it is equal to one, the particles move circularly, and the lower the value, the more elongated the ellipse is.
Even though Array 1 is located in the deep glaciolacustrine basin with the main axis oriented NNW-SSE, we see no or only very mild directionality (Figure 24) - the wavefield is not polarized.

Extraction of dispersion characteristics

We have applied four different approaches to retrieve Rayleigh and Love dispersion curves from the array measurements. Firstly, classical f-k analysis (Capon, 1969; Lacoss et al., 1969) and SPAC (Aki, 1957), both available in the Geopsy package.

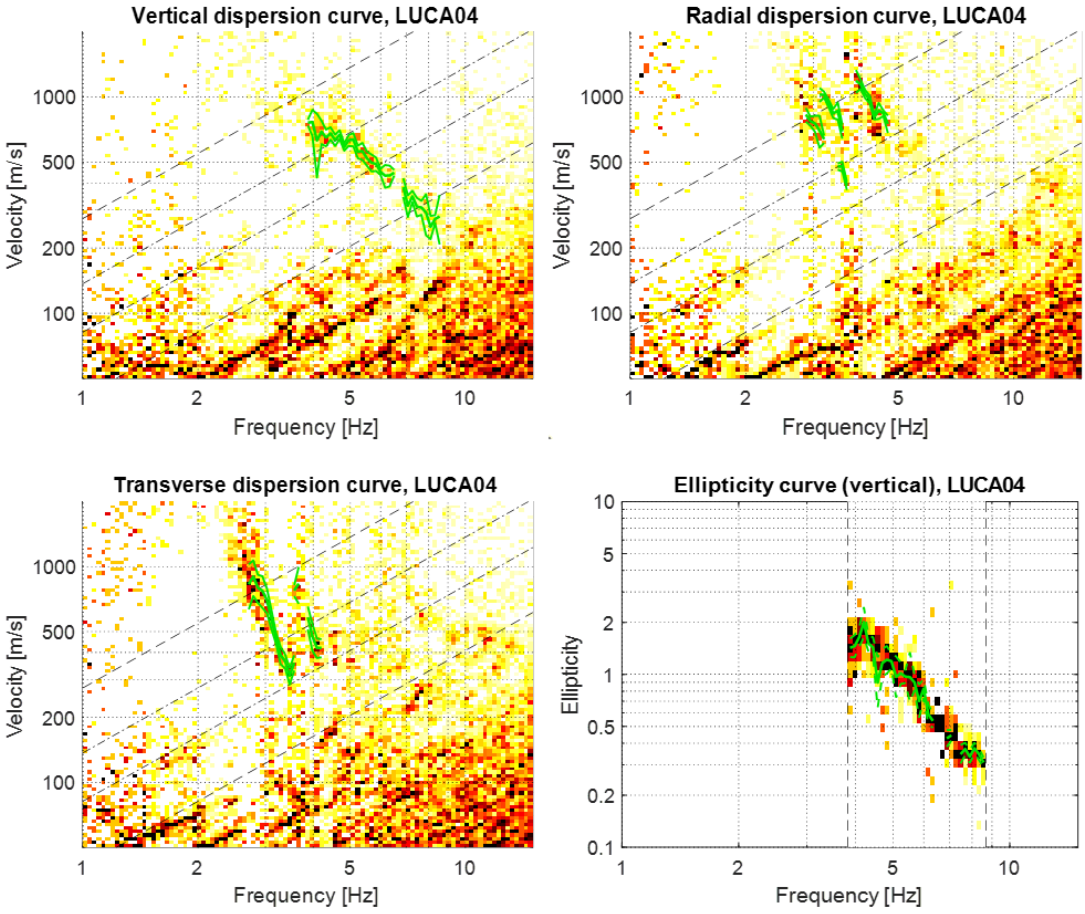

Figure 25. The resulting dispersion curves for Array 4 using 3-component high-resolution f-k. The picked dispersion and ellipticity curves are shown with green lines.

Then, we have applied 3-component high resolution f-k (Poggi et al., 2012a) which allows retrieving vertical, radial and transverse dispersion curves which can be then assigned respectively to Rayleigh and Love waves. In addition, Rayleigh wave ellipticity function, however, with no indication of the sense of particle motion, is extracted. The sense of rotation can be retrieved with WaveDec, which uses wavefield decomposition analysis (Maranò et al., 2017). It provides us directly with Rayleigh and Love dispersion curves, as well as Rayleigh wave ellipticity with a specified prograde or retrograde sense of motion. The results for Array 4 are shown in Figure 25 and Figure 26.

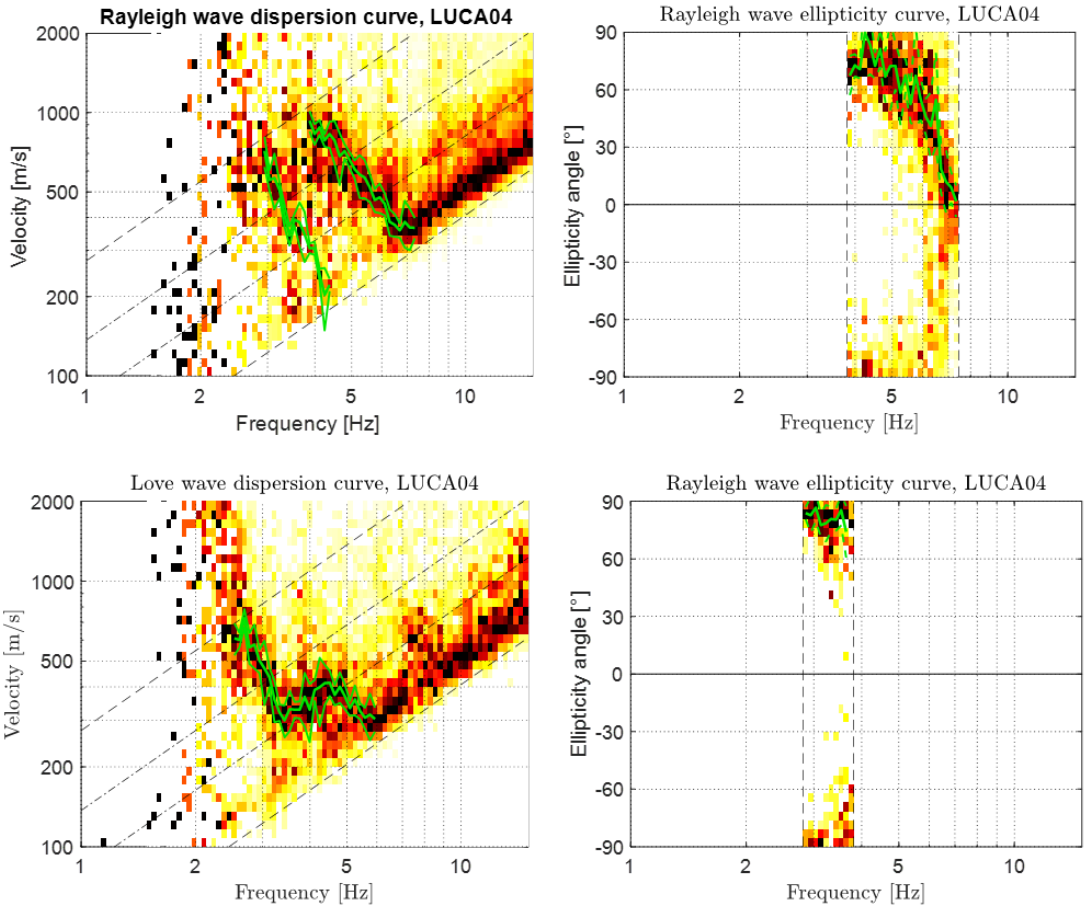

Figure 26. The resulting dispersion curves for Array 4 using WaveDec. The picked dispersion curves and ellipticity angles are shown with green lines.

Picking and mode identification

For all methods, the dispersion curves and their uncertainty are picked (Figure 25 and Figure 26). Figure 27 shows the comparison of all curves for Array 4 adding also the Rayleigh dispersion curves extracted in 2007. The Rayleigh wave ellipticity curves are depicted in terms of ellipticity angle and not dimensionless ellipticity ratio what helps to avoid the problems with possible infinity in ellipticity function during inversion procedure. Because only WaveDec allows distinguishing the sense of motion, the two realisations of other curves (i.e. ellipticity using 3-component FK and RayDec) are plotted.

The next step is mode identification and choosing the target curves for the inversion. For both Love and Rayleigh waves, we can clearly see two modes: fundamental and first higher (Figure 27). For Rayleigh, the fundamental mode is from WaveDec, while the first higher is confirmed by many methods. Opposite for the Love wave, where lower frequency part of first higher mode is visible only from high resolution FK and higher frequency part only using WaveDec, while the fundamental mode is present in each method.

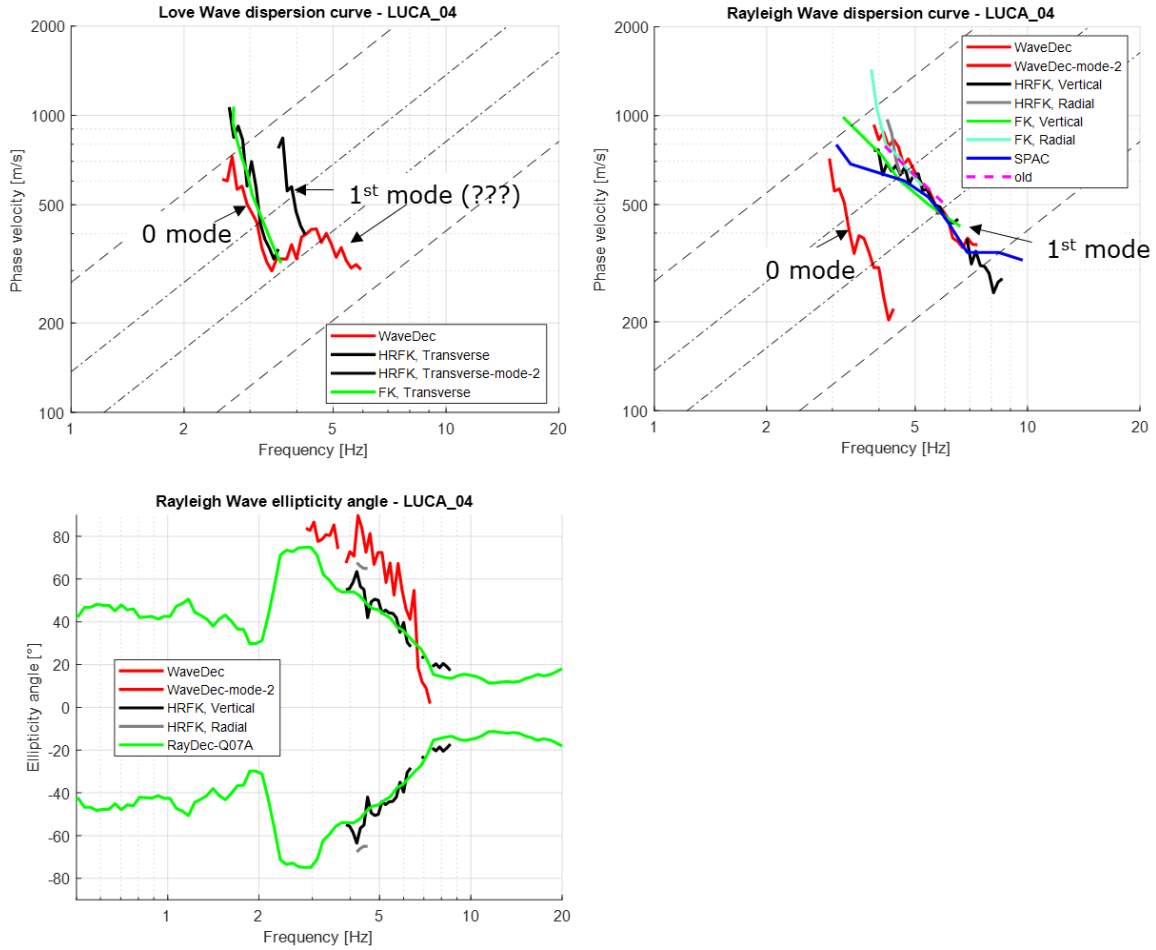

Figure 27. Summary of dispersion curves extracted using different methods for Array 4. The identified modes for Rayleigh and Love waves are marked. Abbreviations: FK – FK algorithm from Geopsy, HRFK – 3-component high-resolution FK (Poggi et al., 2012a), SPAC – SPAC algorithm from Geopsy, WaveDec – wave decomposition method (Maranò et al., 2017), RayDec – a method based on random decrement technique RayDec (Hobiger et al., 2009), old – picking from 2007.

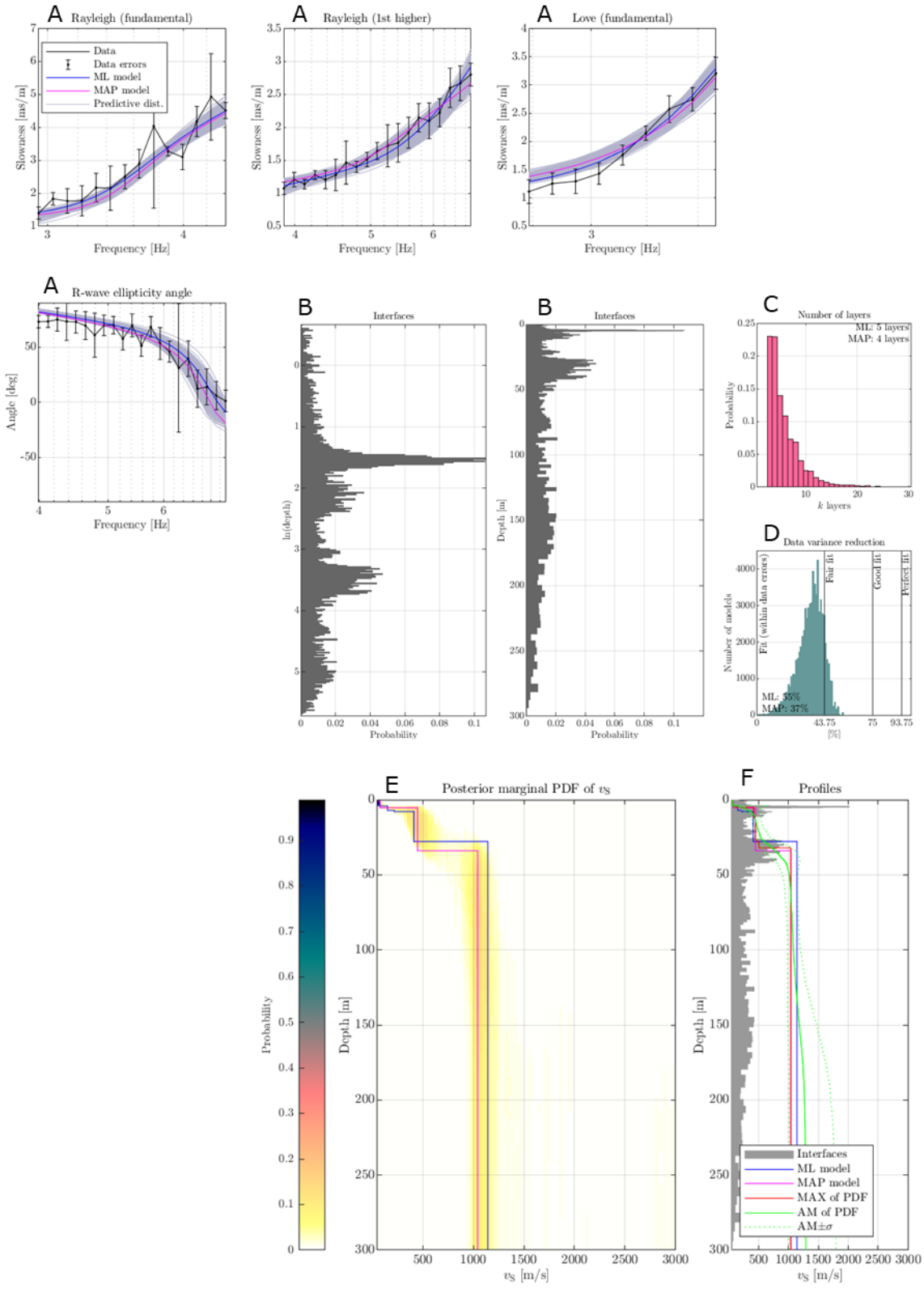

Figure 28. Inversion results using multizonal transdimensional Bayesian inversion (Hallo et al., 2021). The figure shows one of the inversion runs for Array 4. More explanations can be found in the text.

Inversion

We used a novel multizonal transdimensional Bayesian inversion by Hallo et al., (2021) to retrieve the subsoil velocity structure. For each array, we have run several inversions using different parameters and using different dispersion curves as targets. The shown example is one of the runs for Array 4 (Figure 28). The upper plots (A) show dispersion curves in black and all predicted models in grey. The ML and MAP models are blue and pink lines respectively. For Array 4, a relatively good fit is obtained. Plot D shows the data variance reduction, the values are reaching a line indicating "fine fit". The middle plots (B) are histograms of the layer interfaces. The number of layers is a free parameter, while in many algorithms - it is a user choice. The solution from Hallo et al., (2021) is robust and reduces subjectivity. In plot C, the probability of a given number of layers is presented. For Array 4, the ML estimate is 5 and the MAP estimate is 4 layers. Finally, in the E plot, the posterior marginal PDF of shear wave velocity and ML and MAP models are shown. Graph F is again a histogram of layer interfaces plotted together with estimates of shear wave velocity profiles. Based on the presented results, we interpret that below Array 4, the sediment thickness is about 30-35 m and the bedrock shear velocity is about 1100 m/s. Such velocity of the bedrock is supported by similar amplification functions using SSR and empirical spectral modelling methods. The final velocity profile is quite simple, it consists of 3 layers.

5.5.1.3 Urban perspective summary

Several challenges wait for users of ambient vibration array techniques in an urban environment. Firstly, the deployment needs to be planned to take into account the limitation of free-field space in cities and the location of possible strong transient disturbances sources like busy roads, railways, factories, etc. If possible, the measurements should be performed overnight to achieve higher signal quality. Longer recording times than in rural areas are also greatly recommended (a few hours). The quality of the deployment orientation needs to be checked carefully and corrected, because of the higher chance of sensor misorientation in an urban environment. I cannot recommend one specific processing procedure or method that works best in a noisy urban environment. However, the use of many different methods during processing can help to extract more information. For Array 4 (Figure 27), we can retrieve the Rayleigh wave fundamental mode only using the WaveDec method, while the low-frequency part of the first higher mode of Love wave only from the high-resolution FK method. In addition, the usage of a variety of methods helps to verify the result, identify the processing errors, etc.

5.6 Outlook

The results and application of the techniques described in the second part of the report are a part of a detailed site response analysis for the city of Lucerne. An important step of our study will be the development of a 3D velocity model using all geological and geophysical information. It will allow us to apply numerical simulations of earthquake ground motion, or the application of empirical methods to estimate amplification using the quarter-wavelength representation of synthetic velocity profiles extracted from the 3D model or profiles obtained from ellipticity inversion at sites of H/V measurements (Poggi et al., 2012a). Moreover, we will apply among others canonical correlation method by Panzera et al., (2021) to predict the amplification from the H/V ratios. We plan also to study non-linear soil behaviour in the city

of Lucerne. We will take advantage of CPT measurements performed in the area to infer the geotechnical properties (Roten, 2014), as well as a finite-difference code NOAH to simulate the non-linear wave propagation (Bonilla, 2001). The details are to be found in the second deliverable that will be published in 2022.

6. Summary

Site response analysis in any area can be challenging due to complex 2D or 3D wave propagation and possible non-linear soil behaviour, etc. However, densely populated urban areas and industrial environments pose additional difficulties including among other high background noise level hindering usage of empirical seismic methods, the occurrence of strong local sources affecting the application of methods based on ambient noise. In addition, the lack of free space and low security in public areas can make site characterization more difficult. Last but not least, some methods cannot be successfully applied (heavy source active seismic) or are too expensive in an urban environment like the installation of borehole seismic monitoring stations.

I described several methods for site analysis and site characterization indicating the problems that can be encountered in an urban environment. For some of the techniques, I presented very detailed real-life examples from our investigations in the city of Lucerne, including empirical methods and approaches based on ambient vibration. While usage of empirical methods was limited due to a low number of high-quality events recordings and ambient noise methods are hindered due to strong variability of ambient noise wavefield, we achieved the best results using the SSRh method being a combination of both approaches.

In the future, we are going to continue our investigation in the city and neighbouring areas. We plan to expand our study by non-linear soil behaviour modelling which will be the topic of the second deliverable.

Acknowledgments

This PhD project is performed in the framework of the Horizon 2020 ITN funded project URBASIS-EU, which focuses on seismic hazard and risk in urban areas. We would also like to thank Christoph Knellwolf (Verkehr und Infrastruktur, Abteilung Naturgefahren, Kanton Luzern) and the members of SED Engineering Seismology group for their help.

References

Aki, K. (1957). Space and time spectra of stationary stochastic waves, with special reference to microtremors. *Bulletin of the Earthquake Research Institute*, *35*, 415–456.

Alber, J. (2020). *Validation of a three-dimensional geophysical model for the Visp area, Switzerland* [Master Thesis]. ETH Zurich.

Ansal, A. (Ed.). (2015). Chapter 15: A Review and Some New Issues on the Theory of the H/V Technique for Ambient Vibrations. In *Perspectives on European Earthquake Engineering and Seismology: Volume 2* (Vol. 39). Springer International Publishing. https://www.springer.com/gp/book/9783319169637

Antonietti, P. F., Mazzieri, I., Melas, L., Paolucci, R., Quarteroni, A., Smerzini, C., Stupazzini, M., Antonietti, P. F., Mazzieri, I., Melas, L., Paolucci, R., Quarteroni, A., Smerzini, C., & Stupazzini, M. (2021). Three-dimensional physics-based earthquake ground motion simulations for seismic risk assessment in densely populated urban areas. *Mathematics in Engineering*, *3*(2), 1–31. https://doi.org/10.3934/mine.2021012

Arai, H. (2005). S-Wave Velocity Profiling by Joint Inversion of Microtremor Dispersion Curve and Horizontal-to-Vertical (H/V) Spectrum. *Bulletin of the Seismological Society of America*, *95*(5), 1766–1778. https://doi.org/10.1785/0120040243

Arai, H., & Tokimatsu, K. (2004). S-Wave Velocity Profiling by Inversion of Microtremor H/V Spectrum. *Bulletin of the Seismological Society of America*, *94*(1), 53–63. https://doi.org/10.1785/0120030028

Bard, P.-Y. (1997). Local effects of strong ground motion: Basic physical phenomena and estimation methods for microzoning studies. In *SERINA—Seismic Risk: An Integrated Seismological, Geotechnical and Structural Approach* (Institute of Engineering Seismology and Earthquake Engineering (ITSAK), Ministry of Environment and Public Works, pp. 229–299).

Bard, P.-Y. (1999). Microtremor measurements: A tool for site effect estimation? *The Effects of Surface Geology on Seismic Motion*, *3*, 1251–1279.

Bard, P.-Y. (2021, August). Physics-Based Site-Amplification Prediction Equations: A Dream At Reach? *6th IASPEI/IAEE International Symposium: Effects of Surface Geology on Seismic Motion*,. https://hal.archives-ouvertes.fr/hal-03329430

Bard, P.-Y., Acerra, C., Aguacil, G., Anastasiadis, A., Atakan, K., Azzara, R., Basili, R., Bertrand, E., Bettig, B., Blarel, F., Bonnefoy-Claudet, S., Paola, B., Borges, A., Sørensen, M., Bourjot, L., Cadet, H., Cara, F., Caserta, A., Chatelain, J.-L., & Zacharopoulos, S. (2008). Guidelines for the implementation of the H/V spectral ratio technique on ambient vibrations measurements, processing and interpretation. *Bulletin of Earthquake Engineering*, *6*, 1–2.

Beresnev, I. A., & Wen, K.-L. (1996). Nonlinear soil response—A reality? *Bulletin of the Seismological Society of America*, *86*(6), 1964–1978.

Bergamo, P., Hammer, C., & Fäh, D. (2019). *SERA Deliverable D7.4: Improvement of Site Condition Indicators*.

Bergamo, P., Hammer, C., & Fäh, D. (2020). On the Relation between Empirical Amplification and Proxies Measured at Swiss and Japanese Stations: Systematic Regression Analysis and Neural Network Prediction of Amplification. *Bulletin of the Seismological Society of America*. https://doi.org/10.1785/0120200228

Beyreuther, M., Barsch, R., Krischer, L., Megies, T., Behr, Y., & Wassermann, J. (2010). ObsPy: A Python Toolbox for Seismology. *Seismological Research Letters*, *81*(3), 530–533. https://doi.org/10.1785/gssrl.81.3.530

Bonilla, L. F. (2001). *NOAH: User's Manual*.

Bonilla, L. F., Archuleta, R., & Lavallée, D. (2005). Hysteretic and dilatant behavior of cohesionless soils and their effects on nonlinear site response: Field data observations and modeling. *Bulletin of the Seismological Society of America*, *95*, 2373–2395.

Bonilla, L. F., Guéguen, P., & Ben-Zion, Y. (2019). Monitoring Coseismic Temporal Changes of Shallow Material during Strong Ground Motion with Interferometry and Autocorrelation. *Bulletin of the Seismological Society of America*, *109*(1), 187–198. https://doi.org/10.1785/0120180092

Bonilla, L. F., Steidl, J. H., Lindley, G. T., Tumarkin, A. G., & Archuleta, R. J. (1997). Site amplification in the San Fernando Valley, California: Variability of site-effect estimation using the S-wave, coda, and H/V methods. *Bulletin of the Seismological Society of America*, *87*(3), 710–730.

Bonnefoy-Claudet, S., Baize, S., Bonilla, L., Berge-Thierry, C., Pasten, C., Campos, J., Volant, P., & Verdugo, R. (2009). Site effect evaluation in the basin of Santiago de Chile using ambient noise measurements. *Geophysical Journal International*, *176*, 925–937. https://doi.org/10.1111/j.1365-246X.2008.04020.x

Bonnefoy-Claudet, S., Cotton, F., & Bard, P.-Y. (2006). The nature of noise wavefield and its applications for site effects studies: A literature review. *Earth-Science Reviews*, *79*(3), 205–227. https://doi.org/10.1016/j.earscirev.2006.07.004

Bonnefoy-Claudet, S., Köhler, A., Cornou, C., Wathelet, M., & Bard, P.-Y. (2008). Effects of Love Waves on Microtremor H/V Ratio Effects of Love Waves on Microtremor H/V Ratio. *Bulletin of the Seismological Society of America*, *98*(1), 288–300. https://doi.org/10.1785/0120070063

Boudghene Stambouli, A., Zendagui, D., Bard, P.-Y., & Derras, B. (2017). Deriving amplification factors from simple site parameters using generalized regression neural networks: Implications for relevant site proxies. *Earth, Planets and Space*, *69*(1), 99. https://doi.org/10.1186/s40623-017-0686-3

Bradley, B. A. (2015). Correlation of Arias intensity with amplitude, duration and cumulative intensity measures. *Soil Dynamics and Earthquake Engineering*, *78*, 89–98. https://doi.org/10.1016/j.soildyn.2015.07.009

Brune, J. N. (1970). Tectonic stress and the spectra of seismic shear waves from earthquakes. *Journal of Geophysical Research (1896-1977)*, *75*(26), 4997–5009. https://doi.org/10.1029/JB075i026p04997

Burjánek, J., Edwards, B., & Fäh, D. (2014a). Empirical evidence of local seismic effects at sites with pronounced topography: A systematic approach. *Geophysical Journal International*, *197*. https://doi.org/10.1093/gji/ggu014

Burjánek, J., Fäh, D., Pischiutta, M., Rovelli, A., Calderoni, G., & Bard, P.-Y. (2014b). *Site effects at sites with pronounced topography: Overview & recommendations* (Report No. JRA1; Report for EU Project NERA.). ETH Zurich. https://doi.org/10.3929/ethz-a-010222426

Burjánek, J., Gassner-Stamm, G., Poggi, V., Moore, J. R., & Fäh, D. (2010). Ambient vibration analysis of an unstable mountain slope. *Geophysical Journal International*, *180*(2), 820–828. https://doi.org/10.1111/j.1365-246X.2009.04451.x

Capon, J. (1969). High-resolution frequency-wavenumber spectrum analysis. *Proceedings of the IEEE*, *57*(8), 1408–1418. https://doi.org/10.1109/PROC.1969.7278

Castellaro, S., Mulargia, F., & Rossi, P. L. (2008). Vs30: Proxy for Seismic Amplification? *Seismological Research Letters*, *79*(4), 540–543. https://doi.org/10.1785/gssrl.79.4.540

Çelebi, M., Dietel, C., Prince, J., Onate, M., & Chavez, G. (1987). Site Amplification in Mexico City (Determined from 19 September 1985 Strong-Motion Records and from Recordings of Weak Motions). In A. S. Cakmak (Ed.), *Developments in Geotechnical Engineering* (Vol. 44, pp. 141–151). Elsevier. https://doi.org/10.1016/B978-0-444-98956-7.50013-1

Chaljub, E., Celorio, M., Cornou, C., Martin, F. D., Haber, J.-P., Margerin, L., Marti, J., & Zentner, I. (2021, August). Numerical simulation of wave propagation in heterogeneous and random media for site effects assessment in the grenoble valley. *6th IASPEI/IAEE International Symposium: Effects of Surface Geology on Seismic Motion*,.

Chandra, J., Guéguen, P., & Bonilla, L. F. (2016). PGA-PGV/Vs considered as a stress–strain proxy for predicting nonlinear soil response. *Soil Dynamics and Earthquake Engineering*, *85*, 146–160. https://doi.org/10.1016/j.soildyn.2016.03.020

Chávez-García, F. J., Sánchez, L. R., & Hatzfeld, D. (1996). Topographic site effects and HVSR. A comparison between observations and theory. *Bulletin of the Seismological Society of America*, *86*(5), 1559–1573.

Chieppa, D. (2020). *Investigation of the deep subsurface of the Swiss Molasse basin using ambient vibrations and earthquake recordings* [Doctoral Thesis, ETH Zurich]. https://doi.org/10.3929/ethz-b-000462062

Cultrera, G., Cornou, C., Di Giulio, G., & Bard, P.-Y. (2021). Indicators for site characterization at seismic station: Recommendation from a dedicated survey. *Bulletin of Earthquake Engineering*, *19*(11), 4171–4195. https://doi.org/10.1007/s10518-021-01136-7

Curtis, A., Gerstoft, P., Sato, H., Snieder, R., & Wapenaar, K. (2006). Interferometry—Turning noise into signal. *The Leading Edge*, *25*, 1082–1092. https://doi.org/10.1190/1.2349814

Derras, B., Bard, P.-Y., & Cotton, F. (2017). VS30, slope, H800 and f0: Performance of various site-condition proxies in reducing ground-motion aleatory variability and predicting nonlinear site response. *Earth, Planets and Space*, *69*. https://doi.org/10.1186/s40623-017-0718-z

Douglas, J., & Aochi, H. (2008). A Survey of Techniques for Predicting Earthquake Ground Motions for Engineering Purposes. *Surveys in Geophysics*, *29*(3), 187. https://doi.org/10.1007/s10712-008-9046-y

Edwards, B., & Fäh, D. (2013a). A Stochastic Ground-Motion Model for Switzerland. *Bulletin of the Seismological Society of America*, *103*(1), 78–98. https://doi.org/10.1785/0120110331

Edwards, B., & Fäh, D. (2013b). Measurements of stress parameter and site attenuation from recordings of moderate to large earthquakes in Europe and the Middle East. *Geophysical Journal International*, *194*(2), 1190–1202. https://doi.org/10.1093/gji/ggt158

Edwards, B., Michel, C., Poggi, V., & Fäh, D. (2013). Determination of Site Amplification from Regional Seismicity: Application to the Swiss National Seismic Networks. *Seismological Research Letters*, *84*, 611–621. https://doi.org/10.1785/0220120176

Fäh, D., Kind, F., & Giardini, D. (2001). A theoretical investigation of average H/V ratios. *Geophysical Journal International*, *145*(2), 535–549. https://doi.org/10.1046/j.0956-540x.2001.01406.x

Fäh, D., Kind, F., & Giardini, D. (2003). Inversion of local S-wave velocity structures from average H/V ratios, and their use for the estimation of site-effects. *Journal of Seismology*, *7*(4), 449–467. https://doi.org/10.1023/B:JOSE.0000005712.86058.42

Federal Office of Topography swisstopo. (2021). map.geo.admin.ch

Field, E. H. (1996). Spectral amplification in a sediment-filled Valley exhibiting clear basin-edge-induced waves. *Bulletin of the Seismological Society of America*, *86*(4), 991–1005.

Field, E. H., Hough, S., & Jacob, K. H. (1990). Using microtremors to assess potential earthquake site response: A case study in Flushing Meadows, New York City. *Bulletin - Seismological Society of America*, *80*, 1456–1480.

Foti, S., Hollender, F., Garofalo, F., Albarello, D., Asten, M., Bard, P.-Y., Comina, C., Cornou, C., Cox, B., Di Giulio, G., Forbriger, T., Hayashi, K., Lunedei, E., Martin, A., Mercerat, D., Ohrnberger, M., Poggi, V., Renalier, F., Sicilia, D., & Socco, V. (2018). Guidelines for the good practice of surface wave analysis: A product of the InterPACIFIC project. *Bulletin of Earthquake Engineering*, *16*(6), 2367–2420. https://doi.org/10.1007/s10518-017-0206-7

García-Jerez, A., Piña-Flores, J., Sánchez-Sesma, F., Luzon, F., & Perton, M. (2016). A computer code for forward calculation and inversion of the H/V spectral ratio under the diffuse field assumption. *Computers & Geosciences*, *97*, 67–78. https://doi.org/10.1016/j.cageo.2016.06.016

Geoportal Kanton Luzern. (2020). geo.lu.ch

Gisler, M., Fäh, D., & Kästli, P. (2004). Historical seismicity in Central Switzerland. *Eclogae Geologicae Helvetiae*, *97*(2), 221–236. https://doi.org/10.1007/s00015-004-1128-3

Hallo, M., Imperatori, W., Panzera, F., & Fäh, D. (2021). Joint multizonal transdimensional Bayesian inversion of surface wave dispersion and ellipticity curves for local near-surface imaging. *Geophysical Journal International*, *226*(1), 627–659. https://doi.org/10.1093/gji/ggab116

Hobiger, M., Bard, P.-Y., Cornou, C., & Le Bihan, N. (2009). Single station determination of Rayleigh wave ellipticity by using the random decrement technique (RayDec). *Geophysical Research Letters*, *36*, L14303. https://doi.org/10.1029/2009GL038863

Hobiger, M., Bergamo, P., Imperatori, W., Panzera, F., Marrios Lontsi, A., Perron, V., Michel, C., Burjánek, J., & Fäh, D. (2021). Site Characterization of Swiss Strong-Motion Stations: The Benefit of Advanced Processing Algorithms. *Bulletin of the Seismological Society of America*. https://doi.org/10.1785/0120200316

Hobiger, M., Imperatori, W., Bergamo, P., Lontsi, A., Michel, C., & Fäh, D. (2017). *SVEJ: Buochs (NW)—Hafen* [Site Characterization Report]. Swiss Seismological Service (SED).

Imperatori, W., Mai, M., & Fäh, D. (2020, November 7). *SCARF3D: a scalable library to efficiently generate large-scale, three-dimensional random fields*. 18th Swiss Geoscience Meeting 2020, online.

Janusz, P., Perron, V., Imperatori, W., Bonilla, L., & Fäh, D. (2021a, August). Evaluation Of Seismic Site Response In Urban Areas: Insight From The Case Of Lucerne, Switzerland. *The 6th IASPEI / IAEE International Symposium: Effects of Surface Geology on Seismic Motion*.

Janusz, P., Perron, V., Knellwolf, C., Imperatori, W., Bonilla, L., & Fäh, D. (2021b). *Combining recordings of earthquake ground-motion and ambient vibration analysis to estimate site response variability in the city of Lucerne, Switzerland*. EGU General Assembly 2021 (virtual), Vienna, Austria, April 19–30, 2021, online. https://doi.org/10.5194/egusphere-egu21-4380

Jongmans, D., Ohrnberger, M., & Wathelet, M. (2005). *Recommendations for quality array measurements and processing* (Final Report of the SESAME Project No. WP13; Site Effects Assessment Using Ambient Excitations).

Keller + Lorenz AG. (2010). *Baugrund-Hinweiskarte, Blatt 1150 Luzern, Erläuterungen*.

Kind, F., Fäh, D., & Giardini, D. (2005). Array measurements of S-wave velocities from ambient vibrations. *Geophysical Journal International*, *160*(1), 114–126. https://doi.org/10.1111/j.1365-246X.2005.02331.x

Konno, K., & Ohmachi, T. (1998). Ground-motion characteristics estimated from spectral ratio between horizontal and vertical components of microtremor. *Bulletin of the Seismological Society of America*, *88*(1), 228–241.

Kramer, S. L. (1996). *Geotechnical Earthquake Engineering* (1 edition). Pearson.

Lacoss, R. T., Kelly, E. J., & Toksöz, M. N. (1969). Estimation of seismic noise structure using arrays. *GEOPHYSICS*, *34*(1), 21–38. https://doi.org/10.1190/1.1439995

Lermo, J., & Chávez-García, F. J. (1993). Site effect evaluation using spectral ratios with only one station. *Bulletin of the Seismological Society of America*, *83*(5), 1574–1594.

Lermo, J., & Chavez-Garcia, J. (1994). Are microtremors useful in site response evaluation? *Bulletin of the Seismological Society of America*, *84*, 1350–1364.

Lin, C.-P., Lin, C.-H., & Chien, C.-J. (2017). Dispersion analysis of surface wave testing – SASW vs. MASW. *Journal of Applied Geophysics*, *143*, 223–230. https://doi.org/10.1016/j.jappgeo.2017.05.008

Lin, F.-C., Li, D., Clayton, R. W., & Hollis, D. (2012). Interferometry with a dense 3D dataset. In *SEG Technical Program Expanded Abstracts 2012* (Vol. 1–0, pp. 1–6). Society of Exploration Geophysicists. https://doi.org/10.1190/segam2012-0519.1

Liu, P., Archuleta, R. J., & Hartzell, S. H. (2006). Prediction of Broadband Ground-Motion Time Histories: Hybrid Low/High- Frequency Method with Correlated Random Source Parameters. *Bulletin of the Seismological Society of America*, *96*(6), 2118–2130. https://doi.org/10.1785/0120060036

Liu, Y., Li, J., Sun, S., & Yu, B. (2019). Advances in Gaussian random field generation: A review. *Computational Geosciences*, *23*(5), 1011–1047. https://doi.org/10.1007/s10596-019-09867-y

Lobkis, O. I., & Weaver, R. L. (2001). On the emergence of the Green's function in the correlations of a diffuse field. *The Journal of the Acoustical Society of America*, *110*(6), 3011–3017. https://doi.org/10.1121/1.1417528

Maranò, S., Hobiger, M., & Fäh, D. (2017). Retrieval of Rayleigh Wave Ellipticity from Ambient Vibration Recordings. *Geophysical Journal International*, *209*, ggx014. https://doi.org/10.1093/gji/ggx014

Maranò, S., Reller, C., Loeliger, H.-A., & Fäh, D. (2012). Seismic waves estimation and wavefield decomposition: Application to ambient vibrations. *Geophysical Journal International*, *191*(1), 175–188. https://doi.org/10.1111/j.1365-246X.2012.05593.x

Michel, C., Edwards, B., Poggi, V., Burjánek, J., Roten, D., Cauzzi, C., & Fäh, D. (2014). Assessment of Site Effects in Alpine Regions through Systematic Site Characterization of Seismic Stations Assessment of Site Effects in Alpine Regions through Systematic Site Characterization of Seismic Stations. *Bulletin of the Seismological Society of America*, *104*(6), 2809–2826. https://doi.org/10.1785/0120140097

Michel, C., Poggi, V., Cauzzi, C., Burjanek, J., Roten, D., & Fäh, D. (2013). *Lucerne-Bramberg (SLUB)* [Site Characterization Report]. Swiss Seismological Service (SED).

Moczo, P., Kristek, J., Gabriel, A.-A., Chaljub, E., Ampuero, J.-P., Sanchez-Sesma, J., Galis, M., Gregor, D., & Kristekova, M. (2021, August). Numerical Wave Propagation Simulation. *6th IASPEI/IAEE International Symposium: Effects of Surface Geology on Seismic Motion,*.

Nakamura, Y. (1989). A method for dynamic characteristics estimation of subsurface using microtremor on the ground surface. *Railway Technical Research Institute, Quarterly Reports*, *30*(1), 25–33.

Nogoshi, M., & Igarashi, T. (1971). On the Amplitude Characteristics of Microtremor (Part 2). *Zisin (Journal of the Seismological Society of Japan. 2nd Ser.)*, *24*(1), 26–40. https://doi.org/10.4294/zisin1948.24.1_26

Panzera, F., Bergamo, P., & Fäh, D. (2021). Canonical Correlation Analysis Based on Site-Response Proxies to Predict Site-Specific Amplification Functions in Switzerland. *Bulletin of the Seismological Society of America*. https://doi.org/10.1785/0120200326

Paolucci, R., Sangaraju, S., & Smerzini, C. (2021, August). Generating Broadband Ground Motions From Physics-Based Numerical Simulations Using Artificial Neural Networks. *6th IASPEI/IAEE International Symposium: Effects of Surface Geology on Seismic Motion,*.

Park, C., D. Miller, R., & Xia, J. (1999). Multichannel analysis of surface waves (MASW). *Geophysics*, *64*. https://doi.org/10.1190/1.1444590

Parolai, S. (2012). Investigation of site response in urban areas by using earthquake data and seismic noise. *New Manual of Seismological Observatory Practice 2 (NMSOP2)*. https://doi.org/10.2312/gfz.nmsop-2_ch14

Perron, V. (2017). *Apport des enregistrements de séismes et de bruit de fond pour l'évaluation site-spécifique de l'aléa sismique en zone de sismicité faible à modérée* [Doctoral Thesis]. Université Grenoble Alpes.

Perron, V., Gélis, C., Froment, B., Hollender, F., Bard, P.-Y., Cultrera, G., & Cushing, E. M. (2018a). Can broad-band earthquake site responses be predicted by the ambient noise spectral ratio? Insight from observations at two sedimentary basins. *Geophysical Journal International*, *215*(2), 1442–1454. https://doi.org/10.1093/gji/ggy355

Perron, V., Laurendeau, A., Hollender, F., Bard, P.-Y., Gélis, C., Traversa, P., & Drouet, S. (2018b). Selecting time windows of seismic phases and noise for engineering seismology applications: A versatile methodology and algorithm. *Bulletin of Earthquake Engineering*, *16*(6), 2211–2225. https://doi.org/10.1007/s10518-017-0131-9

Picozzi, M., Parolai, S., Bindi, D., & Strollo, A. (2009). Characterization of shallow geology by high-frequency seismic noise tomography. *Geophysical Journal International*, *176*(1), 164–174. https://doi.org/10.1111/j.1365-246X.2008.03966.x

Picozzi, M., Parolai, S., & Kling (Richwalski), S. (2005). Joint inversion of H/V ratios and dispersion curves from seismic noise: Estimating the S-wave velocity of bedrock. *Geophysical Research Letters - GEOPHYS RES LETT*, *32*. https://doi.org/10.1029/2005GL022878

Pitarka, A., & Mellors, R. (2021). Using Dense Array Waveform Correlations to Build a Velocity Model with Stochastic Variability. *Bulletin of the Seismological Society of America*, *111*(4), 2021–2041. https://doi.org/10.1785/0120200206

Poggi, V., Edwards, B., & Fäh, D. (2011). Derivation of a Reference Shear-Wave Velocity Model from Empirical Site Amplification Derivation of a Reference Shear-Wave Velocity Model from Empirical Site Amplification. *Bulletin of the Seismological Society of America*, *101*(1), 258–274. https://doi.org/10.1785/0120100060

Poggi, V., Edwards, B., & Fäh, D. (2012b). The quarter-wavelength average velocity: A review of some past and recent application developments. *Proceedings of 15th World Conference on Earthquake Engineering (15WCEE)*.

15th World Conference on Earthquake Engineering (15WCEE). https://www.research-collection.ethz.ch/handle/20.500.11850/61155

Poggi, V., & Fäh, D. (2010). Estimating Rayleigh wave particle motion from three-component array analysis of ambient vibrations. *Geophysical Journal International*, *180*(1), 251–267. https://doi.org/10.1111/j.1365-246X.2009.04402.x

Poggi, V., & Fäh, D. (2016). *Guidelines and strategies for seismic microzonation in Switzerland* [Report]. SED/ ETH Zurich. https://doi.org/10.3929/ethz-a-010735479

Poggi, V., Fäh, D., Burjanek, J., & Giardini, D. (2012a). The use of Rayleigh-wave ellipticity for site-specific hazard assessment and microzonation: Application to the city of Lucerne, Switzerland. *Geophysical Journal International*, *188*(3), 1154–1172. https://doi.org/10.1111/j.1365-246X.2011.05305.x

Poggi, V., Fäh, D., & Giardini, D. (2013a). Time–Frequency–Wavenumber Analysis of Surface Waves Using the Continuous Wavelet Transform. *Pure and Applied Geophysics*, *170*(3), 319–335. https://doi.org/10.1007/s00024-012-0505-5

Poggi, V., Michel, C., Roten, D., Burjanek, J., Cauzzi, C., & Fäh, D. (2013b). *Lucerne-Werkhofstresse (SLUW)* [Site Characterization Report]. Swiss Seismological Service (SED).

Prieto, G. A., Denolle, M., Lawrence, J. F., & Beroza, G. C. (2011). On amplitude information carried by the ambient seismic field. *Comptes Rendus Geoscience*, *343*(8), 600–614. https://doi.org/10.1016/j.crte.2011.03.006

Prieto, G., & Beroza, G. (2008). Earthquake ground motion prediction using the ambient seismic field. *Geophys. Res. Lett*, *35*. https://doi.org/10.1029/2008GL034428

Prieto, G., Lawrence, J., & Beroza, G. (2009). Anelastic Earth Structure from the Coherency of the Ambient Seismic Field. *Journal of Geophysical Research*, *114*. https://doi.org/10.1029/2008JB006067

Regnier, J. (2021, August). Non-Linear Soil Response At Strong Motion Observation Sites With A Focus On Borehole Array. *6th IASPEI/IAEE International Symposium: Effects of Surface Geology on Seismic Motion,*.

Roten, D. (2014). *Documentation of tools for analysis of nonlinear soil behavior*.

Roten, D., Fäh, D., & Bonilla, L. (2014). Quantification of Cyclic Mobility Parameters in Liquefiable Soils from Inversion of Vertical Array Records. *Bulletin of the Seismological Society of America*, *104*, 3115–3138. https://doi.org/10.1785/0120130329

Roten, D., Fäh, D., & Bonilla, L. F. (2013). High-frequency ground motion amplification during the 2011 Tohoku earthquake explained by soil dilatancy. *Geophysical Journal International*, *193*(2), 898–904. https://doi.org/10.1093/gji/ggt001

Roten, D., Fäh, D., Bonilla, L. F., Alvarez-Rubio, S., Weber, T. M., & Laue, J. (2009). Estimation of non-linear site response in a deep Alpine valley. *Geophysical Journal International*, *178*(3), 1597–1613. https://doi.org/10.1111/j.1365-246X.2009.04246.x

Roten, D., Fäh, D., Cornou, C., & Giardini, D. (2006). 2D resonances in Alpine valleys identified from ambient vibration wavefields. *Geophysical Journal International*, *165*, 889–905. https://doi.org/10.1111/j.1365-246X.2006.02935.x

Sánchez-Sesma, F. J., Rodríguez, M., Iturrarán-Viveros, U., Luzón, F., Campillo, M., Margerin, L., García-Jerez, A., Suarez, M., Santoyo, M. A., & Rodríguez-Castellanos, A. (2011). A theory for microtremor H/V spectral ratio: Application for a layered medium. *Geophysical Journal International*, *186*(1), 221–225. https://doi.org/10.1111/j.1365-246X.2011.05064.x

Schnellmann, M., Anselmetti, F., Giardini, D., McKenzie, J., & Ward, S. (2004). Ancient Earthquakes at Lake Lucerne. *American Scientist*, *92*. https://doi.org/10.1511/2004.1.46

Schnellmann, M., Anselmetti, F. S., Giardini, D., McKenzie, J. A., & Ward, S. N. (2002). Prehistoric earthquake history revealed by lacustrine slump deposits. *Geology*, *30*(12), 1131–1134. https://doi.org/10.1130/0091-7613(2002)030<1131:PEHRBL>2.0.CO;2

Schuster, G. T., Yu, J., Sheng, J., & Rickett, J. (2004). Interferometric/daylight seismic imaging. *Geophysical Journal International*, *157*(2), 838–852. https://doi.org/10.1111/j.1365-246X.2004.02251.x

Schwarz-Zanetti, G., Deichmann, N., Fäh, D., Giardini, D., Jiménez, M., Masciadri, V., Schibler, R., & Schnellmann, M. (2003). The earthquake in Unterwalden on September 18, 1601: A historico-critical macroseismic evaluation. *Eclogae Geol. Helv.*, *96*.

Semblat, J. F. (2011). Modeling Seismic Wave Propagation and Amplification in 1D/2D/3D Linear and Nonlinear Unbounded Media. *International Journal of Geomechanics*, *11*(6), 440–448. https://doi.org/10.1061/(ASCE)GM.1943-5622.0000023

Seyhan, E., Stewart, J. P., & Graves, R. W. (2013). Calibration of a Semi-Stochastic Procedure for Simulating High-Frequency Ground Motions. *Earthquake Spectra*, *29*(4), 1495–1519. https://doi.org/10.1193/122211EQS312M

Shapiro, N. M., Campillo, M., Stehly, L., & Ritzwoller, M. H. (2005). High-Resolution Surface-Wave Tomography from Ambient Seismic Noise. *Science*, *307*(5715), 1615–1618. https://doi.org/10.1126/science.1108339

SIA. (2020). *Actions on Structures, SIA 261*. Swiss Standards, Swiss Society of Engineers and Architects.

Siegenthaler, C., Finger, W., & Kelts, K. (1987). Earthquake and seiche deposits in Lake Lucerne, Switzerland. *Eclogae Geologicae Helvetiae*, *80*(1), 241–260.

Stamm, G., Poggi, V., & Fäh, D. (2008). *Array- und Einzelstationsmessungen in der Stadt Luzern*.

Steidl, J. H., Tumarkin, A. G., & Archuleta, R. J. (1996). What is a reference site? *Bulletin of the Seismological Society of America*, *86*(6), 1733–1748.

Strasser, M., Anselmetti, F. S., Fäh, D., Giardini, D., & Schnellmann, M. (2006). Magnitudes and source areas of large prehistoric northern Alpine earthquakes revealed by slope failures in lakes. *Geology*, *34*(12), 1005–1008. https://doi.org/10.1130/G22784A.1

Swiss Seismological Service (SED). (2021). seismo.ethz.ch

Theodulidis, N., Bard, P.-Y., Archuleta, R., & Bouchon, M. (1996). Horizontal-to-vertical spectral ratio and geological conditions: The case of Garner Valley Downhole Array in southern California. *Bulletin of the Seismological Society of America*, *86*(2), 306–319.

van Ede, M. C., Molinari, I., Imperatori, W., Kissling, E., Baron, J., & Morelli, A. (2020). Hybrid Broadband Seismograms for Seismic Shaking Scenarios: An Application to the Po Plain Sedimentary Basin (Northern Italy). *Pure and Applied Geophysics*, *177*(5), 2181–2198. https://doi.org/10.1007/s00024-019-02322-0

Viens, L., Miyake, H., & Koketsu, K. (2015). Long-period ground motion simulation of a subduction earthquake using the offshore-onshore ambient seismic field. *Geophysical Research Letters*, *42*(13), 5282–5289. https://doi.org/10.1002/2015GL064265

Wapenaar, K., Draganov, D., Snieder, R., Campman, X., & Verdel, A. (2010a). Tutorial on seismic interferometry: Part 1 — Basic principles and applications. *GEOPHYSICS*, *75*(5), 75A195-75A209. https://doi.org/10.1190/1.3457445

Wapenaar, K., & Fokkema, J. (2006). Green's function representations for seismic interferometry. *GEOPHYSICS*, *71*(4), SI33–SI46. https://doi.org/10.1190/1.2213955

Wapenaar, K., Slob, E., Snieder, R., & Curtis, A. (2010b). Tutorial on seismic interferometry: Part 2 — Underlying theory and new advances. *GEOPHYSICS*, *75*(5), 75A211-75A227. https://doi.org/10.1190/1.3463440

Wathelet, M. (2008). An improved neighborhood algorithm: Parameter conditions and dynamic scaling. *Geophysical Research Letters*, *35*(9). https://doi.org/10.1029/2008GL033256

Wathelet, M., Chatelain, J.-L., Cornou, C., Giulio, G. D., Guillier, B., Ohrnberger, M., & Savvaidis, A. (2020). Geopsy: A User-Friendly Open-Source Tool Set for Ambient Vibration Processing. *Seismological Research Letters*. https://doi.org/10.1785/0220190360

Wathelet, M., Jongmans, D., & Ohrnberger, M. (2004). Surface-wave inversion using a direct search algorithm and its application to ambient vibration measurements. *Near Surface Geophysics*, *2*. https://doi.org/10.3997/1873-0604.2004018

Yamanaka, H., Dravinski, M., & Kagami, H. (1993). Continuous measurements of microtremors on sediments and basement in Los Angeles, California. *Bulletin of the Seismological Society of America*, *83*(5), 1595–1609.

Yoshida, N., & Iai, S. (1998). Nonlinear Site Response And Its Evaluation And Prediction. *Proc. 2nd International Symposium on the Effect of Surface Geology on Seismic Motion, Yokosuka, Japan*, 71–90.

Yu, G., Anderson, J. G., & Siddharthan, R. (1993). On the characteristics of nonlinear soil response. *Bulletin of the Seismological Society of America*, *83*(1), 218–244.

Attachment 1

The overview of some available geophysical and geotechnical data in the Lucerne area

Table 1. The list of some available data and past geophysical and geotechnical measurements in the investigated areas.

Type of data	Lucerne, Horw, and Kriens	Starting date / period	Bouchs and Stans	Starting time/period	What is available
Permanent seismic stations	SLUB SLUK SLUW	01.12.2011 02.12.2014 15.12. 2010	SSTS SBUS	13.03.2015 19.05.2019	continuous seismic signal recordings, empirical amplification functions
Ambient noise single stations measurements	213 points	2001-2016	58 points	2014-2017	raw data, H/V curves, fundamental frequency estimates
Array measurements	7 arrays	2007-2012	2 arrays	2017	raw data, dispersion curves, V_s profiles
Active seismic	5 profiles (MASW) 1 downhole	2011	1 downhole	2017	raw data, dispersion curves, V_s profiles
CPT	34 points	2010-2012	1 point	2017	raw data, reports, interpretation
Boreholes	276 points	1968-2011	-	-	geological profiles (images), for some sites - a few geotechnical parameters
Piezometers	6 points	1989-2019	-	-	water table variation (plots)

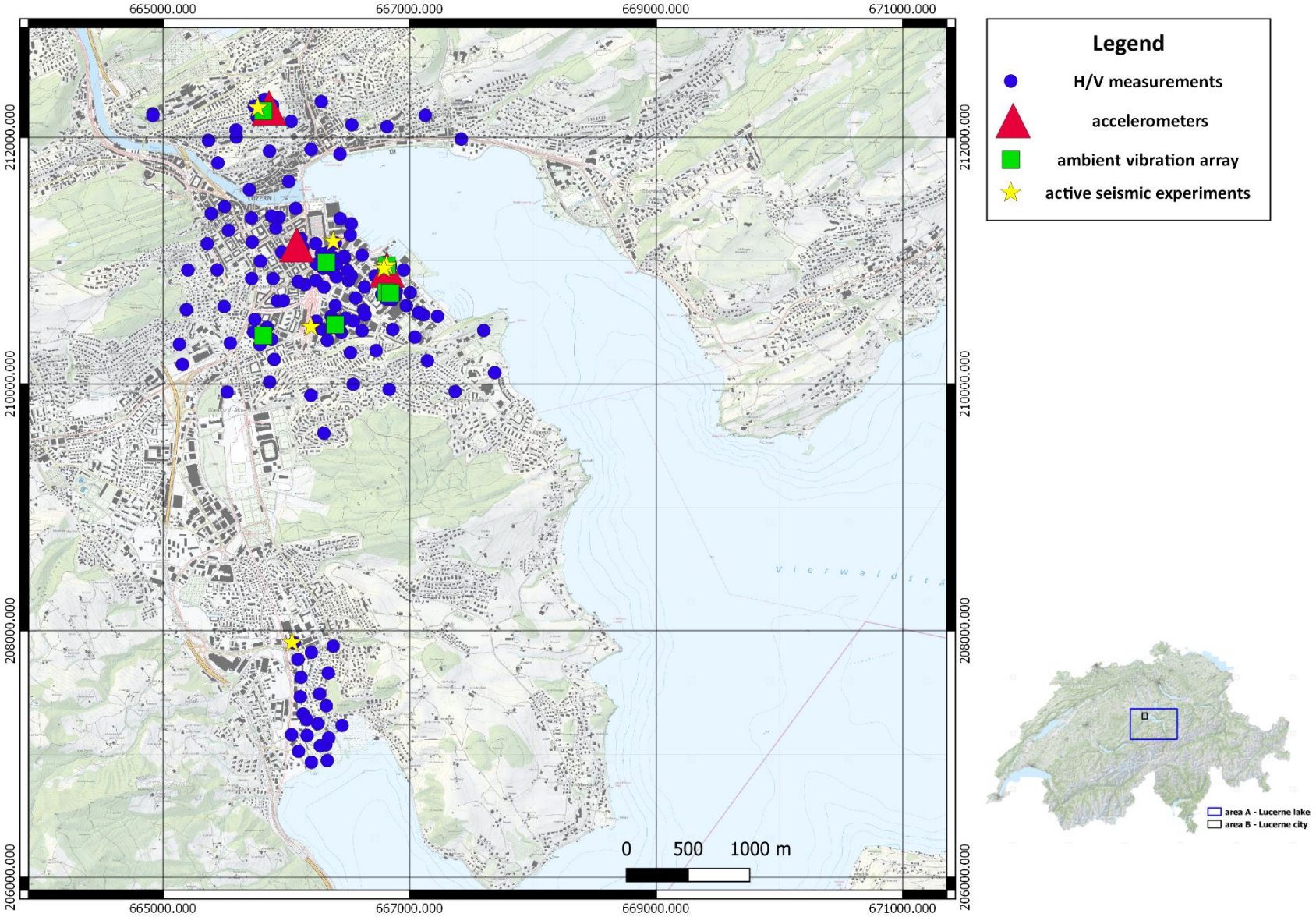

Figure 1. The overview of the past geophysical measurements in the Lucerne city center, Horw, and Kriens. The area showed on the bigger map corresponds to the black rectangular on the map of Switzerland. Base maps source: Federal Office of Topography Swisstopo, (2021).

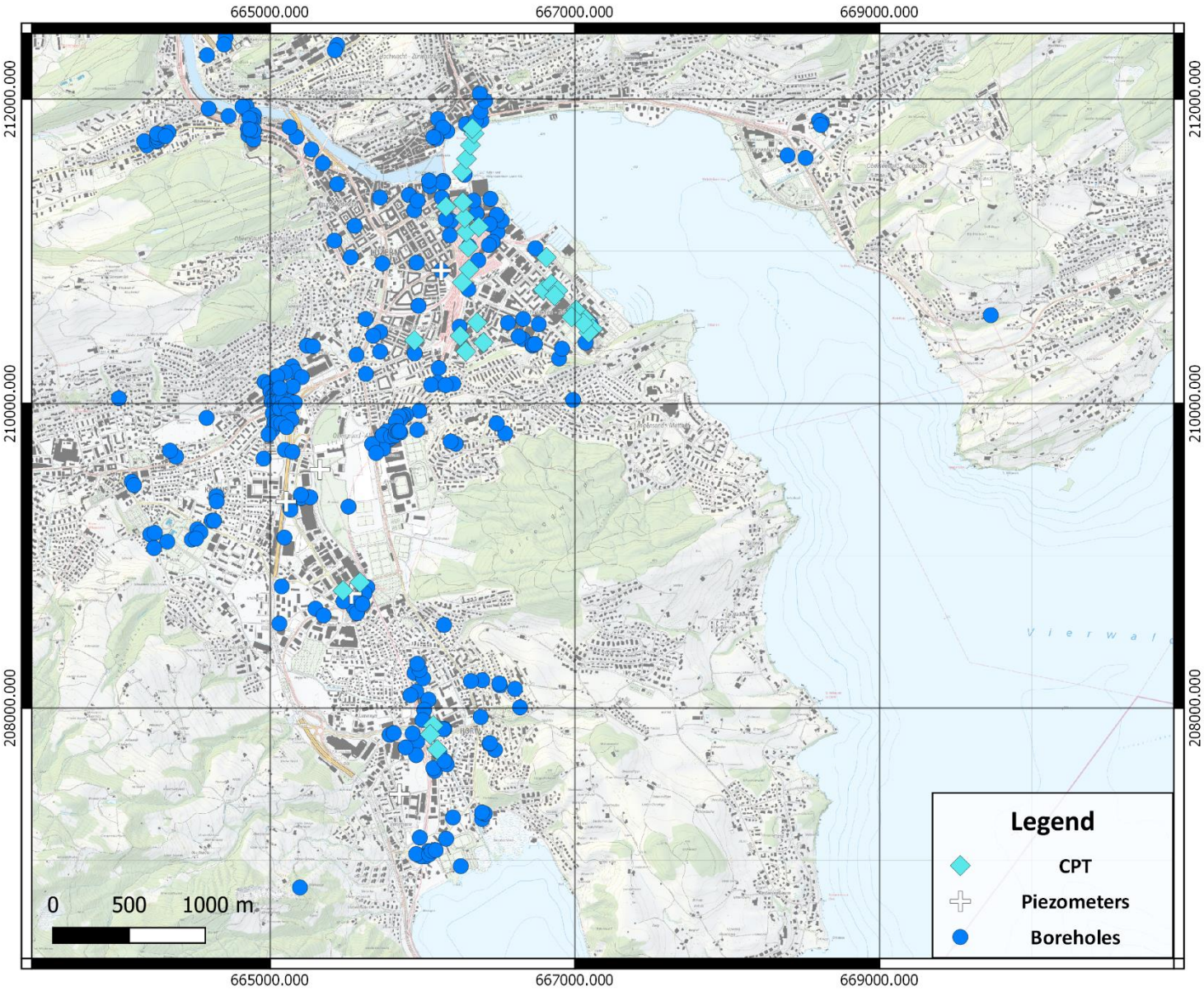

Figure 2. The overview of some available past geotechnical and geological investigations in the Lucerne city center, Horw, and Kriens. Base maps source: Federal Office of Topography Swisstopo, (2021).

Attachment 2

The details of the local temporary seismic network installed in Canton Lucerne and Canton Nidwalden

Table 1. The list of the stations of the local temporary seismic network installed in Canton Lucerne (all but ENE01) and Canton Nidwalden (ENE01). All the stations are short-period seismometers (Lennartz LE-3D/5s) with Centaur digitizer. The table shows the basic information, location, period of recording, etc. Moreover, some basic geological and geotechnical information about the sites is shown (Federal Office of Topography Swisstopo - map.geo.admin.ch). Most of the stations were recording during two separate winter campaigns what is indicated in the 5th and 6th columns. The map below shows the location of the station of the temporary network.

Station code	Station name	Coordinates (CH1903)	Elev. [m]	Start date	End date	Lithology	Soil class	Thickness of unconsolidated deposits [m]	Station class	Station description
LUZ01	Luzern Biregg Schulhaus	666‘512 209‘702	513	28.11.19 08.12.20	14.05.20 06.04.21	siltstone, sandstone, marlstone	A	0	free field	buried sensor, located on a hillside
LUZ02	Luzern Kantonsschule Alpenquai	667‘238 210‘615	436	26.11.19 10.12.20	14.05.20 19.05.21	artificial deposits	D	10-20	free field	buried sensor
LUZ03	Luzern Stadthaus (underground parking)	665‘785 211‘192	436	21.11.19 15.12.20	14.05.20 19.05.21	alluvial deposits	D	35-75	underground shelter	the sensor in an underground shelter (parking) about 5m below the free surface
LUZ04	Luzern Verkehrshaus der Schweiz	668‘225 211‘580	435	26.11.19 15.12.20	14.05.20 06.04.21	alluvial deposits	D	10-20	urban free field	buried sensor, close to the tracks of a small steam train, distance to the building: 5m
LUZ05	Luzern Pfarrei St. Paul	665‘737 210‘364	449	8.12.20	9.04.21	alluvial deposits	C	5-10	free field	a buried sensor placed 1m from the small shed
HOR01	Horw Friedhof Horw	666‘532 207‘917	455	21.11.19 08.12.20	25.06.20 06.04.21	glacial till/ siltstone, sandstone, marlstone	A/E	0-5	free field	buried sensor

HOR02	Horw Seefeld Horw	666‘340 207‘103	435	26.11.19 10.12.20	25.06.20 06.04.21	alluvial deposits	D	100-150	free field	a buried sensor placed 1m from the small shed
HOR03	Horw private house	665‘731 208‘080	446	26.11.19 08.12.20	25.06.20 06.04.21	alluvial deposits	D	100-150	urban free field	buried sensor, located 2m from the one-storey single-family detached house, distance to the building: 2m
KRI01	Kriens Dienststelle MZJ	665‘450 209‘840	456	26.11.19 10.12.20	24.06.20 19.05.21	alluvial deposits	D/E	5-10	free field	buried sensor, surrounded by several high trees
KRI02	Kriens Pfarreiheim Bruder Klaus	664‘756 209‘435	468	28.11.19 08.12.20	25.06.20 06.04.21	alluvial deposits	C	35-50	free field	buried sensor
ENE01	Ennetbürgen Farm/Vorderegg	672‘658 204‘755	889	15.12.20	29.03.21	calcareous marlstone, micrite	A	0	free field	buried sensor, just above solid rock

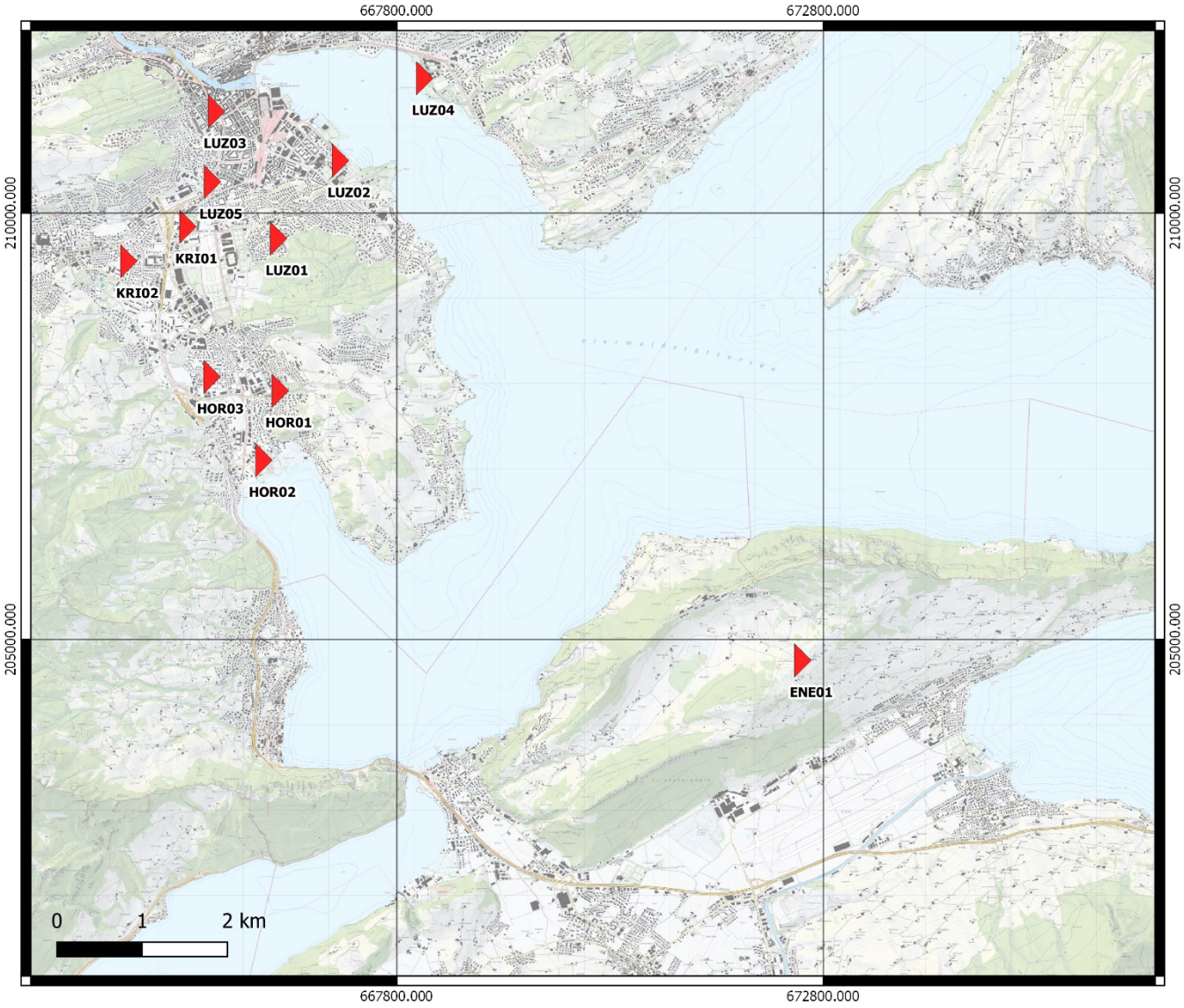

Figure 1. Stations of the temporary network in Canton Lucerne and Canton Nidwalden. Base maps source: Federal Office of Topography Swisstopo, (2021)

Attachment 3

The list of earthquakes recorded by the local temporary seismic network in the Lucerne area.

Table 1. The list of all the earthquakes recorded by the local temporary seismic network in the Lucerne area. Only events, which have a sufficient signal-to-noise ratio to be used in the performed analysis, are listed.

No.	Starting time (GMT)	Origin place	Latitude	Longitude	Magnitude	Depth [km]	Epicentral distance [km]
1	2019-11-26T02:54:12.620000Z	Albania	41.52	19.52	6.4	20	1079
2	2019-11-26T06:08:22.012000Z	Albania	41.58	19.43	5.4	10	1068
3	2019-11-27T07:23:42.552000Z	Crete, Greece	35.73	23.27	6.0	72	1763
4	2019-11-27T14:45:24.434000Z	Albania	41.54	19.47	5.3	13	1074
5	2019-11-26T09:19:26.080000Z	Northwestern Balkan Region	43.24	17.96	5.4	10	863
6	2019-11-30T02:14:45.704610Z	Verbier (VS), Switzerland	46.10	7.30	3.0	4	129
7	2019-12-09T03:37:05.390000Z	Central Italy	43.99	11.31	4.6	10	409
8	2020-01-28T19:10:24.963000Z	Cuba Region	19.42	-78.76	7.7	15	8227
9	2020-01-24T17:55:13.987000Z	Turkey	38.39	39.09	6.7	10	2669
10	2020-01-28T20:15:08.171000Z	Albania	41.47	19.54	5.1	10	1084
11	2020-01-30T11:21:37.234000Z	Dodecanese Islands, Greece	35.23	27.81	5.8	10	2083
12	2020-01-25T19:07:43.302808Z	Realp (UR), Switzerland	46.61	8.46	2.4	6	47
13	2020-01-25T19:13:28.756778Z	Graechen (VS), Switzerland	46.24	7.72	3.0	4	99
14	2020-01-27T22:05:41.108176Z	Albstadt, Germany	48.30	8.95	3.5	7	150
15	2020-02-14T03:13:05.634198Z	Binn (VS), Switzerland	46.34	8.13	2.4	6	77
16	2020-03-25T02:49:20.896000Z	East of Kuril Islands	48.97	157.69	7.5	55	8940
17	2020-03-21T00:49:51.451000Z	Greece-Albania Border Region	39.37	20.63	5.7	10	1308
18	2020-03-22T05:24:03.700000Z	Northwestern Balkan Region	45.91	15.97	5.3	10	598

19	2020-03-22T06:01:20.679000Z	Northwestern Balkan Region	45.91	15.98	4.6	10	598
20	2020-03-18T01:54:57.057565Z	Montreux (VD), Switzerland	46.48	7.00	2.7	9	118
21	2020-04-23T21:52:40.988023Z	Steckborn (TG), Switzerland	47.61	8.97	2.6	0	83
22	2020-05-02T12:51:06.662000Z	Crete, Greece	34.21	25.71	6.6	17	2036
23	2020-05-18T23:22:35.293000Z	Crete, Greece	34.22	25.52	5.8	10	2023
24	2020-05-20T23:43:18.178000Z	Central Mediterranean Sea	35.16	20.29	5.7	20	1652
25	2020-06-23T06:25:41.127671Z	Chamonix, France	46.04	6.92	3.8	5	153
26	2020-12-28T05:28:07.913000Z	Northwestern Balkan Region	45.44	16.19	4.8	10	629
27	2020-12-29T11:19:54.771000Z	Northwestern Balkan Region	45.43	16.26	6.4	10	635
28	2020-12-30T05:15:04.495000Z	Northwestern Balkan Region	45.47	16.18	4.8	5	627
29	2020-12-30T05:26:42.200000Z	Northwestern Balkan Region	45.53	16.17	4.7	10	624
30	2021-01-06T17:01:43.684000Z	Northwestern Balkan Region	45.43	16.24	4.7	10	633
31	2021-01-05T00:46:25.743208Z	Goeschenen (UR), Switzerland	46.68	8.54	1.5	8	41
32	2021-01-05T00:48:06.861427Z	Goeschenen (UR), Switzerland	46.68	8.54	1.7	8	41
33	2021-02-10T13:19:55.905000Z	Southeast of Loyalty Islands	-23.05	171.60	7.7	10	16961
34	2021-02-17T03:36:07.081000Z	Greece	38.41	22.02	5.5	5	1468
35	2021-02-03T22:35:36.860227Z	Bern	46.98	7.44	2.8	4	68
36	2021-02-05T14:14:11.661805Z	Singen, Germany	47.75	8.83	3.2	11	90
37	2021-02-07T09:37:20.715010Z	Neuchatel, Switzerland	47.04	7.01	2.9	-1	101
38	2021-02-14T23:11:04.474313Z	Unterschaechen (UR), Switzerland	46.89	8.83	2.1	8	41
39	2021-03-03T10:16:10.197000Z	Greece	39.76	22.18	6.3	10	1376
40	2021-03-04T18:38:19.350000Z	Greece	39.78	22.12	5.8	10	1371
41	2021-03-18T00:04:06.798000Z	Northern Algeria	36.92	5.20	6.0	8	1152
42	2021-03-27T13:47:55.771000Z	Adriatic Sea	42.44	16.07	5.5	10	794
43	2021-03-01T19:43:36.475270Z	Steckborn (TG), Switzerland	47.69	9.06	3.1	22	93

44	2021-03-15T13:27:35.630776Z	Bern, Switzerland	46.89	7.42	3.2	5	71
45	2021-03-25T03:38:56.997902Z	Unterschaechen (UR), Switzerland	46.90	8.82	1.5	3	40
46	2021-04-06T08:54:21.510000Z	Northwestern Balkan Region	45.22	16.29	4.7	10	645